Heterogeneity and mitochondrial vulnerability configurate the divergent immunoreactivity of human induced microglia-like cells

米元, 耕輔

Clinical Immunology 255 (2023) 109756

Contents lists available at ScienceDirect

Clinical Immunology

journal homepage: www.elsevier.com/locate/yclim

Heterogeneity and mitochondrial vulnerability configurate the divergent immunoreactivity of human induced microglia-like cells

Kousuke Yonemoto [a], Fumihiko Fujii [a], Ryoji Taira [a], Masahiro Ohgidani [b,c], Katsuhide Eguchi [a], Sayaka Okuzono [a,d], Yuko Ichimiya [a], Yuri Sonoda [a], Pin Fee Chong [a], Hironori Goto [a], Hikaru Kanemasa [a], Yoshitomo Motomura [a], Masataka Ishimura [a], Yuhki Koga [a], Keita Tsujimura [e,f], Takao Hashiguchi [g], Hiroyuki Torisu [d], Ryutaro Kira [h], Takahiro A. Kato [b], Yasunari Sakai [a,*], Shouichi Ohga [a]

[a] Department of Pediatrics, Graduate School of Medical Sciences, Kyushu University, Fukuoka, Japan
[b] Department of Neuropsychiatry, Graduate School of Medical Sciences, Kyushu University, Fukuoka, Japan
[c] Department of Functional Anatomy and Neuroscience, Asahikawa Medical University, Hokkaido, Japan
[d] Section of Pediatrics, Department of Medicine, Fukuoka Dental College, Fukuoka, Japan
[e] Group of Brain Function and Development, Neuroscience Institute of the Graduate School of Science, Nagoya University, Aichi, Japan
[f] Research Unit for Developmental Disorders, Institute for Advanced Research, Nagoya University, Aichi, Japan
[g] Laboratory of Medical Virology, Institute for Life and Medical Sciences, Kyoto University, Kyoto, Japan
[h] Department of Pediatric Neurology, Fukuoka Children's Hospital, Fukuoka, Japan

ARTICLE INFO

Keywords:
Microglia
Immunoreactivity
Heterogeneity
Divergence
Mitochondria
and CD14

ABSTRACT

Microglia play versatile roles in progression of and protection against neuroinflammatory diseases. Little is known, however, about the mechanisms underlying the diverse reactivity of microglia to inflammatory conditions. We investigated how human induced microglia-like (iMG) cells respond to innate immune ligands. Quantitative PCR showed that poly-I:C and lipopolysaccharide (LPS) activated the expression of *IL1B* and *TNF*. Immunoreactivity of iMG did not differ between controls ($n = 11$) and patients with neuroinflammatory diseases ($n = 24$). Flow cytometry revealed that $CD14^{high}$ cells expressed interleukin (IL) -1β after LPS treatment. Immunoblotting showed that poly-I:C and LPS differentially activated inflammatory pathways but commonly induced mitochondrial instability and the expression of *pyruvate kinase isoform M2 (PKM2)*. Furthermore, a potent stimulator of PKM2 (DASA-58) alleviated IL-1β production after LPS treatment. These data indicate that heterogeneous cell populations and mitochondrial stability underlie the divergent immunoreactivity of human iMG in environments.

1. Introduction

Microglia are yolk sac-derived resident macrophages in the central nervous system (CNS) [18,27,58]. As a family of phagocytic cells, microglia refine the connectivity of neurons through synaptic pruning, thus configuring the critical period for learning and synaptic plasticity early in childhood [3,44,50].

As antigen-presenting cells in the brain, microglia also play versatile roles in the progression of and protection against neuroinflammatory diseases (NIDs), such as acute encephalopathy [15,26,28] and acquired demyelinating syndromes (ADS), in childhood [5,7,45,59]. In ADS, early demyelinating lesions are characterized by the infiltration of microglia, peripheral macrophages, T-cells, and plasma cells [21,23]. "Classically activated" microglia in these lesions are critical for the phagocytosis of myelin, antigen presentation to T-cells, and release of proinflammatory cytokines [13,21], whereas "alternatively activated"

Abbreviations: ADS, acquired demyelinating syndromes; AESD, acute encephalopathy with biphasic seizures and late reduced diffusion; CNS, central nervous system; ΔΨm, Mitochondrial inner membrane potential; iMG, induced microglia-like cells; iMφ, induced macrophage-like cells; NIDs, neuroinflammatory diseases; PKM2, pyruvate kinase isoform M2; ROS, Reactive oxygen species.

* Corresponding author at: Department of Pediatrics, Graduate School of Medical Sciences, Kyushu University, 3-1-1 Maidashi, Higashi-ku, Fukuoka 812-8582, Japan.
E-mail address: sakai.yasunari.530@m.kyushu-u.ac.jp (Y. Sakai).

https://doi.org/10.1016/j.clim.2023.109756
Received 1 June 2023; Accepted 2 September 2023
Available online 9 September 2023

microglia are crucial for clearing myelin debris and carrying out remyelination [21,23].

The dichotomy of microglial functions helps us simplify their complex phenotypes under variable environmental conditions [46]. However, increasing evidence shows that the human brain consists of microglia with temporarily and spatially heterogeneous populations [32,54]. These data indicate that microglia support the postnatal development of the human brain with diverse susceptibility to inflammatory and degenerative diseases [20].

Until recently, there have been obstacles hampering the investigation of the functional roles of microglia in the human brain and establishment of experimental models using patient-derived cells. However, induced pluripotent stem (iPS) cells and brain organoids have contributed to the recapitulation of the pathogenic conditions of microglia with human cells [42]. More recently, the single-cell RNA sequencing system has unraveled the human-specific heterogeneity of microglia [33].

Both ADS and acute encephalopathy are NIDs that develop in otherwise healthy children and adults [22,61]. Various genetic and environmental factors are known to be associated with these conditions; however, details concerning critical microbes or deficits in the host immunity remain elusive [2,8,31]. To explore the functional roles of microglia in patients, we have recently developed an *in vitro* differentiation system of induced microglia-like (iMG) cells from human peripheral monocytes [39,40]. According to transcriptomic analyses, iMG cells show distinct gene expression profiles according to the culture condition [57]. Thus, monocyte-derived iMG are capable of recapitulating both resting and activated states of microglia in surgically resected tissues from a patient's brain [57].

Using this approach, we investigated how iMG from patients with NIDs respond to innate immune ligands. We herein report that iMG from children with NIDs and those from healthy adults are indistinguishable from each other in terms of the gene expression and cytokine production

Table 1
Summary of monocytes and induced microglia-like cells from participants in this study.

No	Subject	Sex	Diagnosis	Category	Age [a]		Monocyte	
					Onset	Sampling	N (x10^5 cells)	$CD14^{high}$ (%)
1	AE-PT1	M	AESD	Patient	0y8m	7y	28.0	94.50
2	AE-PT2	M	AE	Patient	2y11m	14y	13.2	96.55
3	AE-PT3	M	AE	Patient	0y11m	8y	6.6	91.33
4	AE-PT4	F	AESD	Patient	1y5m	13y	9.1	96.32
5	AE-PT5	M	AESD	Patient	1y0m	10y	6.0	97.10
6	AE-PT6	F	AE	Patient	0y1m	8y	12.0	94.27
7	AE-PT7	F	AESD	Patient	1y0m	5y	4.0	95.25
8	AE-PT8	M	AE	Patient	3y10m	6y	5.7	96.04
9	AE-PT9	M	AE	Patient	1y5m	13y	11.4	81.02
10	AE-PT10	F	AESD	Patient	0y11m	4y	15.0	96.01
11	AE-PT11	M	AE	Patient	13y	13y	125	99.22
12	AE-PT12	F	AESD	Patient	2y8m	12y	25.0	95.88
13	AE-PT13	F	AESD	Patient	0y4m	9y	5.8	98.87
14	AE-PT14	M	GVHD	Patient	14y	14y	5.6	86.76
15	AE-PT15	F	AESD	Patient	1y1m	14y	18.0	96.21
16	AE-PT16	F	AESD	Patient	1y7m	4y	7.8	90.55
17	AE-PT17	M	AE	Patient	0y5m	7y	13.7	97.21
18	AE-PT18	F	AE	Patient	2y2m	5y	4.4	86.78
19	AE-PT19	F	AE	Patient	0y4m	9y	5.2	88.61
20	AE-PT20	F	OMAS	Patient	1y9m	9y	10.8	96.22
21	AE-CT3	M	EP	Control	8y8m	17y	6.0	94.14
22	AE-CT4	M	EP	Control	2y5m	15y	4.8	95.36
23	AE-CT5	M	NMOSD	Patient	8y3m	20y	70.0	95.63
24	MS-PT1	M	MOGAD	Patient	7y5m	13y	14.3	89.76
25	MS-PT2	M	MS	Patient	23y4m	38y	38.0	97.23
26	SSPE-1	M	SSPE	Patient	10y7m	23y	4.0	94.56
27 [b]	AE-HC24	M		Control		34y	5.4	97.54
28	AE-HC27	M		Control		32y	5.8	95.10
29	AE-HC28	M		Control		37y	8.0	93.02
30	AE-HC29	M		Control		35y	10.0	94.16
31	AE-HC30	M		Control		32y	3.5	96.96
32	AE-HC32	M		Control		30y	11.2	91.71
33	AE-HC33	M		Control		34y	26.0	95.53
34	AE-HC38	M		Control		31y	26.8	88.29
35	AE-HC39	M		Control		42y	43.2	92.17
36 [c]	AE-HC11	M		Control		40y	22.4	97.37
37	AE-HC12	M		Control		47y	19.2	75.73
38	AE-HC13	M		Control		41y	13.6	90.69
39	AE-HC14	M		Control		60y	19.2	89.30
40	AE-HC15	M		Control		40y	7.4	93.85
41	AE-HC16	M		Control		20y	25.6	94.03
42	AE-HC17	M		Control		49y	27.2	95.19
43	AE-HC26	M		Control		32y	9.9	92.41
44	AE-HC40	F		Control		37y	11.5	94.51
45	AE-HC41	F		Control		41y	22.7	93.56
46	AE-HC42	F		Control		36y	18.7	94.06

AE = acute encephalitis/encephalopathy with unknown etiology; AESD = acute encephalopathy with biphasic seizures and late reduced diffusion; EP = epilepsy; GVHD = graft versus host disease; MOGAD = myelin oligodendrocyte glycoprotein antibody-associated disease; MS = multiple sclerosis; NMOSD = neuromyelitis optica spectrum disorders; OMAS = opsoclonus myoclonus ataxia syndrome; SSPE = subacute sclerosing panencephalitis.

[a] Age represents years (y) and months (m).

[b] Sample No. 27-35 (healthy adults) were used for optimizing the protocol.

[c] Sample No. 36-46 (healthy adults) were used for subsequent analyses.

after stimulations with polyinosine-deoxycytidylic acid (poly-I:C) and lipopolysaccharide (LPS). Flow cytometry and immunofluorescence studies provide evidence that their diverse reactivities correspond to the ratio of $CD14^{high}CD11^{dim}$ to $CD14^{dim}$ $CD11^{high}$ cells. LPS and poly-I:C distinctively activate their downstream pathways in iMG, whereas both ligands commonly disrupt the mitochondrial inner membrane potential. Furthermore, a chemical stimulator of pyruvate kinase isoform M2 (PKM2) reduces the inflammatory response of iMG. These data indicate that the heterogeneity of iMG correlates with the divergent immunoreactivity of individuals to environmental stresses.

2. Materials and methods

2.1. Participants

Participants were children (<18 years of age at onset) who received diagnoses of and treatments for ADS, acute encephalopathy, and encephalitis at Kyushu University Hospital from 2012 to 2022 (Table 1). A total of 24 patients with NIDs were enrolled in this study. One patient (MS-PT2) developed multiple sclerosis at age 23 years during the follow-up for primary immunodeficiency in our hospital. His blood was sampled at age 38 years. As non-inflammatory disease controls, 2 children with epilepsy were recruited (sampling age: 15 and 17 years old, both male). Twenty adults (sampling age: 20 to 60 years, 17 males and 3 females) were recruited as healthy controls.

2.2. iMG cells

Human blood-derived iMG were prepared as previously described [40]. In brief, peripheral blood was collected in a heparinized tube from pediatric patients (5–10 mL) and adults (20 mL). Peripheral blood mononuclear cells were isolated by a density gradient centrifugation with Histopaque-1077 (#10771; Sigma-Aldrich, St. Louis, MO, USA). CD11b-positive monocytes were bead-purified with the magnetic cell-sorting kit (#130–049-601; Miltenyi Biotec, Bergisch Gladbach, Germany). The isolated cells were resuspended in a conical tube containing RPMI-1640 (#11875093; Thermo Fisher Scientific, Waltham, MA, USA), 10% heat-inactivated fetal bovine serum (FBS), and 1% Penicillin-Streptomycin (#26253–84; Nacalai Tesque, Kyoto, Japan) and plated in culture chambers at 2×10^5 cells/mL. Cells were then cultured overnight under standard conditions (37 °C, 5% CO_2). After overnight incubation, non-adherent cells were removed from the culture media. To develop iMG cells, the adherent monocytes were cultured with RPMI-1640 Glutamax (#61870036; Thermo Fisher Scientific) supplemented with 1% Antibiotic-Antimycotic (#15240062; Thermo Fisher Scientific), 10 ng/mL recombinant human GM-CSF (#215-GM-010; R&D Systems, Minneapolis, MN, USA), and 100 ng/mL recombinant human interleukin (IL) -34 (#5265-IL-010; R&D Systems) for 14 days. To obtain induced macrophage-like (iMφ) cells, the adherent monocytes were cultured with RPMI-1640 Glutamax supplemented with 1% Antibiotic-Antimycotic and 10 ng/mL recombinant human GM-CSF for 14 days. To activate iMGs cells, 50 μg/mL poly-I:C (#tlrl-pic; InvivoGen) and 1 μg/mL LPS (#L2630; Sigma) was added to the culture medium for 3 h (flow cytometry) or 24 h (other assays). All *in vitro* assays were performed at or before 21 days after introduction. To accelerate tetramer formation of PKM2, iMG cells were treated with 50 μM 3-(4-(2,3-dihydrobenzo[b][1,4]dioxin-6-ylsulfonyl)-1,4-diazepan-1-ylsulfonyl) aniline (DASA-58, #SML2853-5MG; Sigma-Aldrich) for 1 h before stimulation with LPS and poly-I:C [43]. To block the co-stimulatory function of CD14, iMG cells were pretreated with 5 μg/mL atibuclimab (#SML2853-5MG; MedChemExpress, Monmouth Junction, NJ, USA) for 1 h before addition of LPS [16]. Human IgG4 isotype control recombinant antibody (#403701; BioLegend, San Diego, CA, USA) was used as a negative control.

2.3. Cell lines

THP-1 cells were purchased from JCRB Cell Bank (#JCRB0112; National Institutes of Biomedical Innovation, Health and Nutrition, Osaka, Japan) [38]. The cells were cultured in RPMI-1640, 10% heat-inactivated fetal bovine serum (FBS) and 1% Penicillin-Streptomycin at 37 °C in 5% CO_2. THP-1 cells were activated with 100 nM phorbol-12-myristate-13-acetate (PMA) for 3 h. All assays were performed at passages 7 to 18.

2.4. Quantitative real-time polymerase chain reaction (PCR)

After incubation with poly-I:C or LPS for 24 h, total RNA was extracted with an RNeasy Micro Kit (#74004; Qiagen, Venlo, Netherlands) and complementary DNA was synthesized using a High-Capacity RNA to cDNA Kit (#4387406; Thermo Fisher Scientific) according to the manufacturer's protocol. Assays were carried out using the SYBR green system (#4385612; Thermo Fisher Scientific). The delta-delta cycle threshold method was applied for the quantitative measurement of gene expression [1]. Human *actin-beta* (*ACTB*) was used as an internal control. Sequences of oligonucleotide primers are provided in Table S1.

2.5. Cytokine assays

After incubation with poly-I:C or LPS for 24 h, conditioned media were centrifuged at 10,000 rpm for 10 min and kept frozen at −80 °C. The levels of pro- and anti-inflammatory cytokines (IL-6, IL-8, IL-1β, and tissue necrosis factor-alpha [TNFα]) were measured by the Cytometric Beads Array system (#551811; Becton, Dickinson and Company, Franklin Lakes, NJ, USA). Undetectable levels of IL-1β were further analyzed with an ultra-sensitive electrochemiluminescence method (S-PLEX platform #K151ADSS; Meso Scale Diagnostics, Rockville, MD, USA).

2.6. Flow cytometry

Cultured cells were washed two times with phosphate-buffered saline (PBS; pH 7.4), and then detached using Cell Dissociation Solution, non-enzymatic (#03–071-1B; Biological Industries Ltd., Beit-Haemek, Israel). The cells were collected by centrifugation at 300G for 5 min and suspended in MACS Buffer. For extracellular staining, the cells were incubated with primary antibodies conjugated to fluorochrome for 30 min at room temperature. For intracellular staining, cells were incubated with 1 μg/mL LPS and 10 μg/mL Brefeldin A (#inh-bfa; InvivoGen) for 3 h, collected, and permeabilized with PerFix-nc Kit (#B31167; Beckman-Coulter, Inc., Brea, CA, USA). Flow cytometry was performed using a EC800 flow cytometer (#EC800; Sony Biotechnology Inc., San Jose, CA, USA) [53]. Data were analyzed with the Kaluza Analysis Software program, ver. 2.1 (#B16406; Beckman Coulter). Antibodies used in the present study are shown in Table S2.

2.7. Immunofluorescence

Cells were inoculated on a Cell Desk LF-1 (MS-92132; Sumitomo Bakelite, Tokyo, Japan), fixed with 4% paraformaldehyde (PFA), and permeabilized with 0.1% Triton X-100 as previously described [1]. Samples were then blocked with blocking buffer (0.1% Triton X-100, 3% FBS) and incubated overnight at 4 °C in the presence of 1 μg/mL primary antibodies. Alexa 488-, 555-, and 647-labelled anti-rabbit, mouse, and chicken antibodies (#A28180, #A27034, and #A21449, respectively; Thermo Fisher Scientific) were used as the secondary antibodies. The fluorescence dye, 4′,6-diamidino-2-phenylindole (DAPI) was used for nuclear staining. Confocal images were obtained with A1 HD25 (Nikon Inc., Tokyo, Japan), as previously described. Phase contrast images and fluorescent images were taken with the all-in-one microscope BZ-X800

equipped with the analytical software program BZ-X (Keyence, Osaka, Japan). For quantitative measurements of nuclear and whole-cell signals of PKM2, the mean fluorescent intensity of the immuno-labelled protein in each region of interest (ROI) was measured using the ImageJ software (version 1.54f, 29 June 2023).

2.8. Western blotting

Standard methods were used as previously described [1]. In brief, cells were grown on a 6-well plate at 2×10^5 cells/mL. The cells were washed with cold PBS and lysed on ice with TES-T buffer: 150 mM NaCl, 2 mM EDTA, 20 mM Tris-HCl (pH 7.5), and 1% Triton X-100 supplemented with protease inhibitor cocktail (#11873580 001; Roche Diagnostics, Basel, Switzerland) and phosphatase inhibitor cocktail (#04906845001; Roche Diagnostics). Laemmli sampling buffer (#161–0747; BioRAD, Hercules, CA, USA) containing 2-mercaptoethanol (1%) was added to whole-cell lysates. Equivalent protein amounts from boiled samples were separated by sodium dodecyl sulfate-polyacrylamide gel electrophoresis (SDS-PAGE) using 4–15% Mini-PROTEAN TGX Gels (#4561083, #4561084 and #4561085; BioRAD). The blotted membranes were blocked with 5% milk and incubated overnight at 4 °C with primary antibodies (Table S2). The membranes were then washed for 10 min with PBS supplemented with 0.05% Tween-20 (PBS-T) 3 times and incubated with peroxidase-conjugated monoclonal mouse anti-rabbit IgG (#170–6515; BioRAD) or goat anti-mouse IgG (#170–6516; BioRAD) for 2 h at room temperature. Chemiluminescence signals were detected using the FluorChem FC2 System (ProteinSimple, San Jose, CA, USA). For quantitative measurements of protein expression, ACTB was used as an internal control.

2.9. Mitochondrial inner membrane potential (ΔΨm)

The ΔΨm was measured using the MitoProbe JC-1 Assay Kit (#M34152; Thermo Fisher Scientific) [55]. The stimulated cells were incubated with 2 μM 5′,6,6′-tetrachloro-1,1′,3,3′-tetraethylbenzimidazolylcarbocyanine iodide (JC-1) at 37 °C for 30 min and labelled with Annexin V (#88–8007-72; Thermo Fisher Scientific). Cells were then gently detached from the bottom of 6-well plates and subjected to flow cytometry. JC-1 monomers (depolarized, green) and aggregates (polarized, orange-red) were observed with excitation/emission settings of 488/530 nm and 540/595 nm, respectively. As a positive control, cells were soaked in 50 μM carbonyl cyanide 3-chlorophenylhydrazone (CCCP) at 37 °C for 5 min before JC-1 labelling [25].

2.10. Reactive oxygen species (ROS)

To measure mitochondrial ROS in iMG, the stimulated cells were stained with 2.5 μM MitoSOX (#M36008; Thermo Fisher Scientific) at 37 °C for 5 min [55]. Cells were detached from the 6-well plates and analyzed by flow cytometry using 488-nm excitation. For positive controls, cells were treated with 5 μM CCCP for 24 h prior to MitoSOX labelling.

2.11. Statistics

Statistical analyses were performed with R ver. 4.2 (http://R-project.org) and JMP software ver. 16 (SAS Institute, Cary, NC, USA). Wilcoxon's signed-rank and rank sum tests were used for the analysis of nonparametric paired and unpaired datasets, respectively. A multiple comparison analysis was performed with Bonferroni's correction. *P* values of <0.05 were considered significant.

2.12. Ethics

This study was conducted in stringent compliance with the institutional guideline for clinical studies using human samples. The protocol was approved by the institutional review board at Kyushu University (#28–88, 29–393 and 678–01). Informed consent was obtained from the parents of each patient and healthy adults prior to the acquisition of blood samples.

3. Results

3.1. Establishment of iMG from pediatric patients

To establish iMG from pediatric patients, we first optimized the differentiation system with small-scale blood sampling from 9 healthy adults (Fig. 1A). From 10 to 20 mL of peripheral blood samples, 3.5 to 125×10^5 CD11b-positive monocytes were obtained. We then consecutively established iMG from a total of 24 patients with NIDs (sampling age: 4 to 38 years, 13 males [54%]) (Table 1). Among them, 9 patients received the diagnosis of acute encephalopathy with biphasic seizures and late reduced diffusion (AESD) [36,56,61], 9 with unclassified acute encephalopathy or encephalitis, 3 with ADS [5], and 3 with other NIDs (one with graft-*versus*-host disease [GVHD], one with opsoclonus myoclonus ataxia syndrome, and one with subacute sclerosing panencephalitis [SSPE]). Two patients with epilepsy were assigned to the control group. Because of the minimal blood sampling performed, however, we were unable to establish iMφ from pediatric patients for a pairwise analysis of phenotypes with those of iMG.

Subsets of monocytes are known to differentially react with immune ligands [52]. We therefore analyzed the monocyte lineage with the conventional algorithm [24]. Based on the expression of pattern recognition receptor CD14 [64] and Fc gamma III receptor CD16 [65] on the surface of monocytes, we classified the monocytes into classical ($CD14^{high}$ CD16-), nonclassical ($CD14^{dim}$ CD16+), and intermediate ($CD14^{high}$ CD16+) subsets (Fig. 1B). Monocytes from patients with NIDs and controls showed similar proportions of the classical (median 85.8% *vs.* 83.2%), nonclassical (4.77% *vs.* 4.12%), and intermediate subsets (7.53% *vs.* 11.2%; $p = 0.195$, 0.775, and 0.175, respectively; Wilcoxon's rank sum test) (Fig. 1C).

During 14 days of differentiation *in vitro* (div), monocytes gained the mature morphology of iMG with a ramified structure and expanded cell soma (Fig. 1D, **S1A, B**). By Day 14 div, iMG cells began to express the microglia-specific markers TMEM119, P2RY12, and CX3C motif chemokine receptor 1 (CX3CR1) (Fig. 1E), indicating that iMG in our experimental system reproduced phenotypes equivalent to those in previous studies [39,40,57].

3.2. Heterogeneous cell population of iMG

We examined the differential expression of surface markers between iMG and iMφ cells. According to the expression profiles of these myeloid markers, iMG were classified into two subgroups: $CD14^{high}$ $CD11b^{dim}$ and $CD14^{dim}CD11b^{high}$ cells (Fig. 1F). Because of minimal blood sampling, flow cytometry was performed only for one pediatric patient (AE-PT11) and 14 adults (Tables S3, S4). Thus, data on subpopulation of $CD14^{high}$ cells in iMGs were not available for all pediatric samples. As described in previous studies [40], iMG showed a higher CD11b and lower CD14 expression than did iMφ (Fig. 1F, G). In this system, iMG showed a marginally lower rate of $CD14^{high}$ cells than iMφ ($p = 0.0625$, Wilcoxon's signed-rank test; Fig. 1G, **S1C**). The population ratios of $CD11b^{high}$ and $CD45^{high}$ cells in iMG were similar to those in iMφ ($p = 0.312$ and 0.625, respectively; Wilcoxon's signed-rank test; Fig. 1G, **S1C**). The ratios of $CD14^{high}CD11b^{dim}$ cell populations in iMG were not correlated with the age of participants ($n = 16$, Pearson's correlation coefficients, Fig. 1H). These data suggested that peripheral monocytes differentiated into iMG consisting of heterogeneous cell populations.

3.3. Transcriptional activation and cytokine releases from iMG cells

We wondered whether iMG from children with NIDs show higher

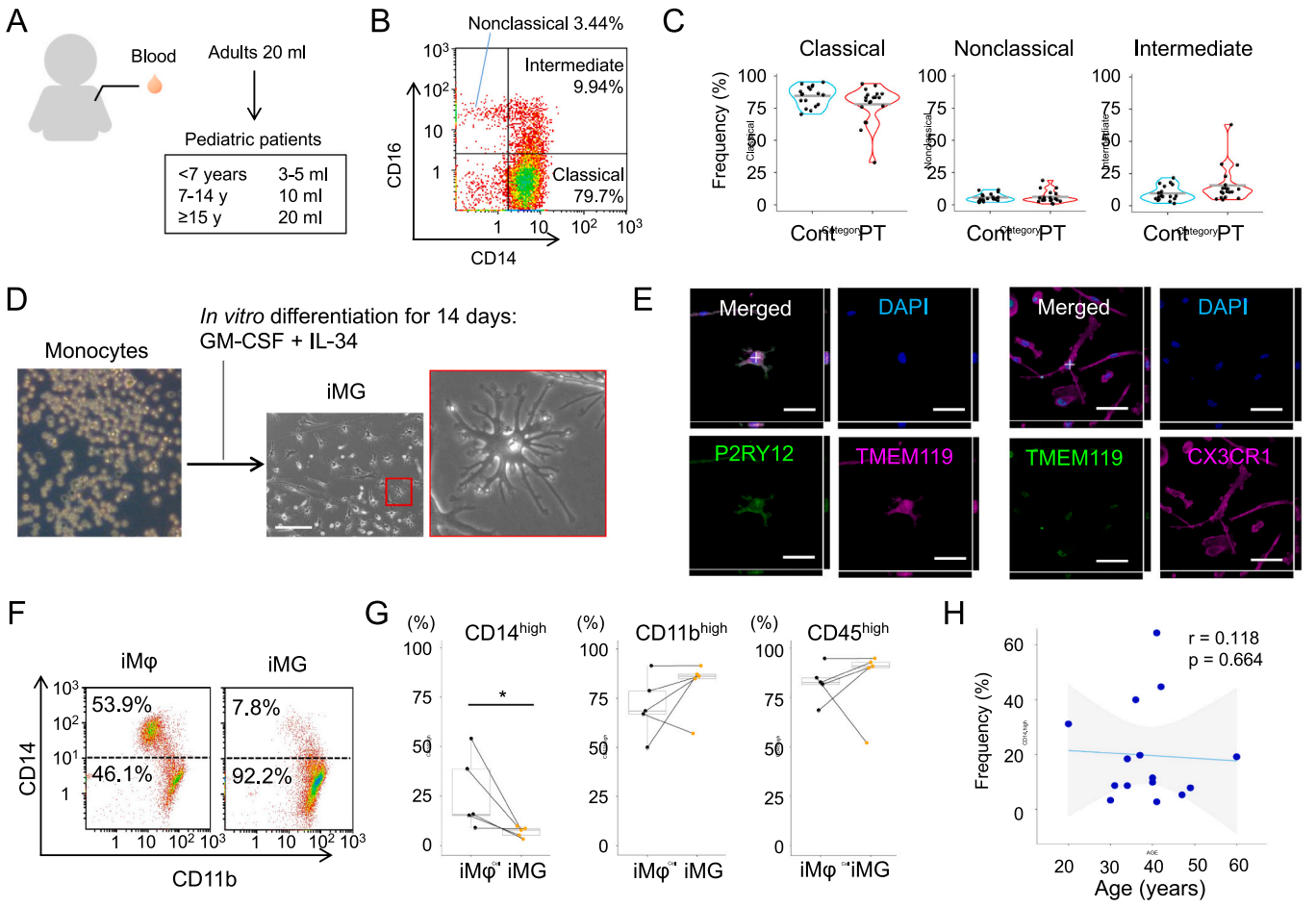

Fig. 1. Establishment of induced microglia-like cells from pediatric patients

(A) Blood sampling from healthy adults and pediatric patients. The sampling volume was adjusted to 3–5 mL (under age 7 years), 5–10 mL (7–14 years) and 20 mL (≥15 years).

(B) A subset analysis of monocytes. According to the expression of CD14 and CD16, monocytes were classified into classical ($CD14^{high}$ $CD16^{-}$; right-lower), nonclassical ($CD14^{dim}$ $CD16^{+}$; left-upper), and intermediate ($CD14^{high}$ $CD16^{+}$; right-upper) subtypes.

(C) A comparison of the subtype population in monocytes from pediatric patients with NIDs (red, $n = 24$) and controls (blue, $n = 11$). *$P < 0.05$ (Wilcoxon's rank sum test). "Cont" and "PT" represent controls and patients, respectively.

(D) *In vitro* differentiation of monocytes into induced microglia-like (iMG) cells. Microscopic appearance of iMG before and after differentiation with GM-CSF and IL-34. Scale bar, 200 μm.

(E) The expression of microglial markers in iMG. Cross symbol indicates the point of optical slices for the XZ and YZ planes of confocal images. Scale bar, 50 μm.

(F) The expression of myeloid markers (CD11b and CD14) on iMG and induced macrophage-like (iMφ) cells.

(G) The decreased expression of CD14 and unremarkable changes in expression of CD11b and CD45 on iMG compared to those on iMφ. *P < 0.05 ($n = 5$ each, Wilcoxon's signed-rank test).

(H) Variable expression of CD14 in iMG from participants at different ages ($n = 16$). R and p values were obtained from Pearson's correlation analysis.

reactivities to immune ligands than those from control subjects. To clarify this point, we determined the expression of transcripts encoding proinflammatory cytokines before and after treatment with the innate immune ligands, poly-I:C and LPS. Quantitative (q) PCR revealed that both ligands robustly increased the expression of *TNF* ($p = 9.54 \times 10^{-7}$ [poly-I:C] and 3.05×10^{-5} [LPS]) and *IL1B* ($p = 2.86 \times 10^{-6}$ [poly-I:C] and 3.05×10^{-5} [LPS], Wilcoxon's signed-rank test; Fig. 2A, top). Similarly, poly-I:C and LPS increased the expression of *SLC1A2* and *SLC1A3*, the two genes encoding glutamate transporters (EAAT2 and EAAT1), compared to the basal condition ($p = 6.1 \times 10^{-5}$ [poly-I:C] and 1.95×10^{-3} [LPS], respectively; Wilcoxon's signed-rank test; Fig. 2A, middle). Of note, poly-I:C treatment, but not LPS treatment, activated the transcription of type I interferon-coding genes *IFNA1* and *IFNB1* (Fig. 2A, bottom).

We then measured cytokines in culture media before and after poly-I:C and LPS treatment. Both treatments similarly increased the level of TNFα, IL-6, and IL-8 (Fig. 2B). In this assay, however, IL-1β remained under the detection limit after the treatments. Thus, we determined the concentration of IL-1β in culture media with an ultrasensitive system (S-Plex), which confirmed the increase in IL-1β concentrations after LPS treatment (median 2720.0 *vs.* 0.1 ng/mL ; $p = 4.82 \times 10^{-6}$; Wilcoxon's rank sum test; Fig. 2C, **S2**). However, no significant difference was found in the cytokine levels between iMG from patients and those from healthy controls (Fig. 2B, C).

Although we did not detect any hyperactive immune responses of iMG from children with NIDs compared with those from controls, we observed that iMG from all participants showed distinct patterns of responses to LPS from those to poly-I:C. In Western blotting, LPS induced the expression of pro-IL-1β, whereas poly-I:C did not show this effect (Fig. 2D). In this system, Poly-I:C, but not LPS, increased the expression of STAT1, a downstream effector of the type I interferon-dependent pathway [19].

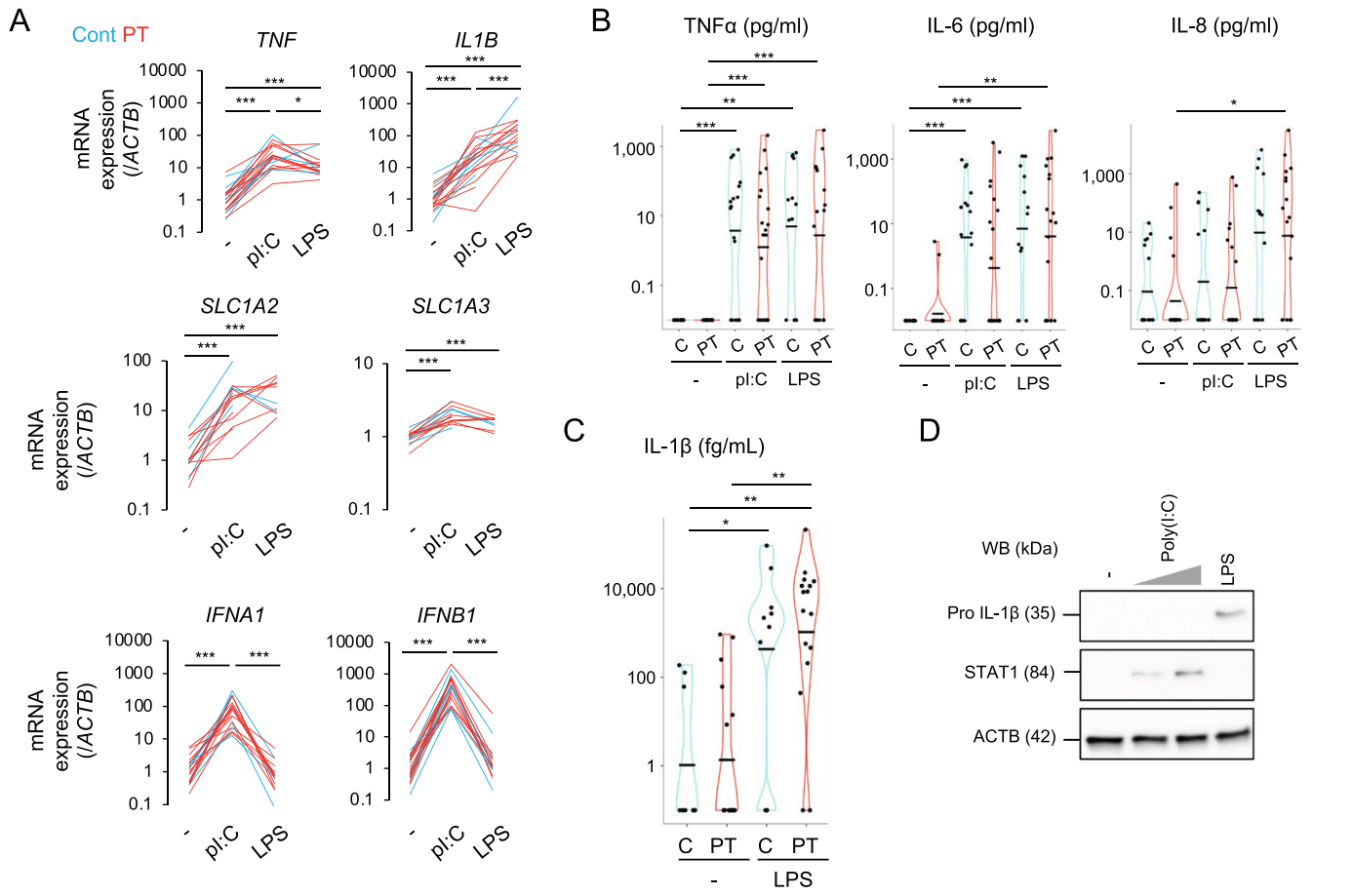

Fig. 2. Diverse reactivity of iMG from different individuals

(A) The relative expression of cytokine- and glutamate transporter-encoding genes in iMG after poly-I:C and LPS treatment (24 h). Line plots show quantitative PCR data for patients with NIDs (red: PT) and controls (blue: Cont). Each line denotes one subject. The expression levels of the gene indicated at top are shown as relative values to those without treatments (−). For panels A-C, pI:C and LPS labels represent treatments with poly-I:C and LPS, respectively; and the minus (−) indicates no treatment. *P < 0.05, **$p < 0.01$ and ***$p < 0.001$ (*TNF, IL1B, IFNA1 and IFNB1*: $n = 21$, 21 and 16; *SLC1A2* and *SLC1A3*: $n = 15$, 15 and 10, respectively; Wilcoxon's signed-rank test).

(B) Cytokines in the culture media. Dots show the concentration of each cytokine before (−) and after treatment with poly-I:C ($n = 35$) and LPS ($n = 29$) for 24 h. Each dot denotes one subject. For panels B and C, labels of "C" and "PT" represent controls and patients, respectively.

(C) Measurement of IL-1β concentrations in culture media with a high-sensitivity method, S-Plex ($n = 25$). Each dot denotes one subject.

(D) Differential responses of iMG to poly-I:C and LPS treatments. Representative Western blotting for iMG from a healthy adult (HC26). The panels show that pro-IL-1β and STAT1 were distinctively expressed after treatment with LPS (1 μg/mL) and poly-I:C (5 μg/mL and 50 μg/mL) for 24 h.

3.4. Distinctive molecular pathways activated by poly-I:C and LPS

To test whether distinctive molecular pathways were activated by poly-I:C and LPS, we compared the expression profiles of nuclear factor-kappa B (NF-κB)-dependent genes (*IL1B* and *TNF*) and type I interferon-coding genes (*IFNA1* and *IFNB1*) in iMG from each individual. We confirmed that the expression of *IL1B* was correlated with that of *TNF* (Pearson's correlation analysis; Fig. 3A, left). Similarly, the expression of *IFNA1* and *IFNB1* was correlated with each other after poly-I:C treatment (Fig. 3A, right-upper). In contrast, the expression of neither *IFNA1* nor *IFNB1* was correlated with that of the NF-κB-dependent genes *TNF* and *IL1B* (Fig. 3A, middle, **S3A**). No correlation was observed in either the combination of *IFNA1-IL1B*, *IFNB1-ILB1*, or *IFNB1-TNF* (**Fig. S3A**). We further confirmed that the concentrations of NF-κB-associated cytokines (IL-6, IL-8, and TNFα) were correlated with each other in culture media (**Fig. S3B**). These data recapitulated the notion that poly-I:C and LPS activate distinctive molecular pathways downstream to Toll-like receptor 3 (TLR3) and 4 (TLR4), respectively (Fig. 3C). We further hypothesized that both the heterogeneity of the cell population and diversity among individuals contributed to the variable reactivity of human iMG to LPS and poly-I:C.

3.5. Heterogeneous reactivities of iMG to innate immune ligands

TLR4 recognizes LPS with an essential aid of CD14, a glycophosphatidylinositol (GPI)-anchored protein [64], thereby inducing NF-κB-responsive genes, *IL1B* and *TNF* [66]. We therefore wondered whether the expression of *IL1B* and *TNF* was correlated with that of CD14 in iMG. However, neither the expression of *IL1B* nor *TNF* after treatment with LPS was significantly correlated with that of CD14 (Pearson's correlation analysis; Fig. 4A).

To obtain direct evidence concerning the expression of IL-1β protein in CD14-expressing ($CD14^{high}$) cells, we performed a flow cytometric analysis with intracellular immunolabelling with anti-pro-IL-1β before and after treatment with LPS. We confirmed that IL-1β- and TNFα-expressing (+) cells were increased after LPS treatment (Fig. 4B). As expected, the expression of IL-1β was restricted to the subpopulation of $CD14^{high}$ cells (86.9%), whereas TNF-α was expressed in both $CD14^{high}$ (86.8%) and $CD14^{dim}$ cells (56.5%) after LPS treatment (Fig. 4C). The frequency of IL-1β + cells was correlated with that of $CD14^{high}$ cells (Fig. 4D, upper). However, no such correlation was observed in the relationship between TNFα and CD14 (Fig. 4D, lower). We further excluded the possibility that the frequency of $CD14^{high}$ cells did not

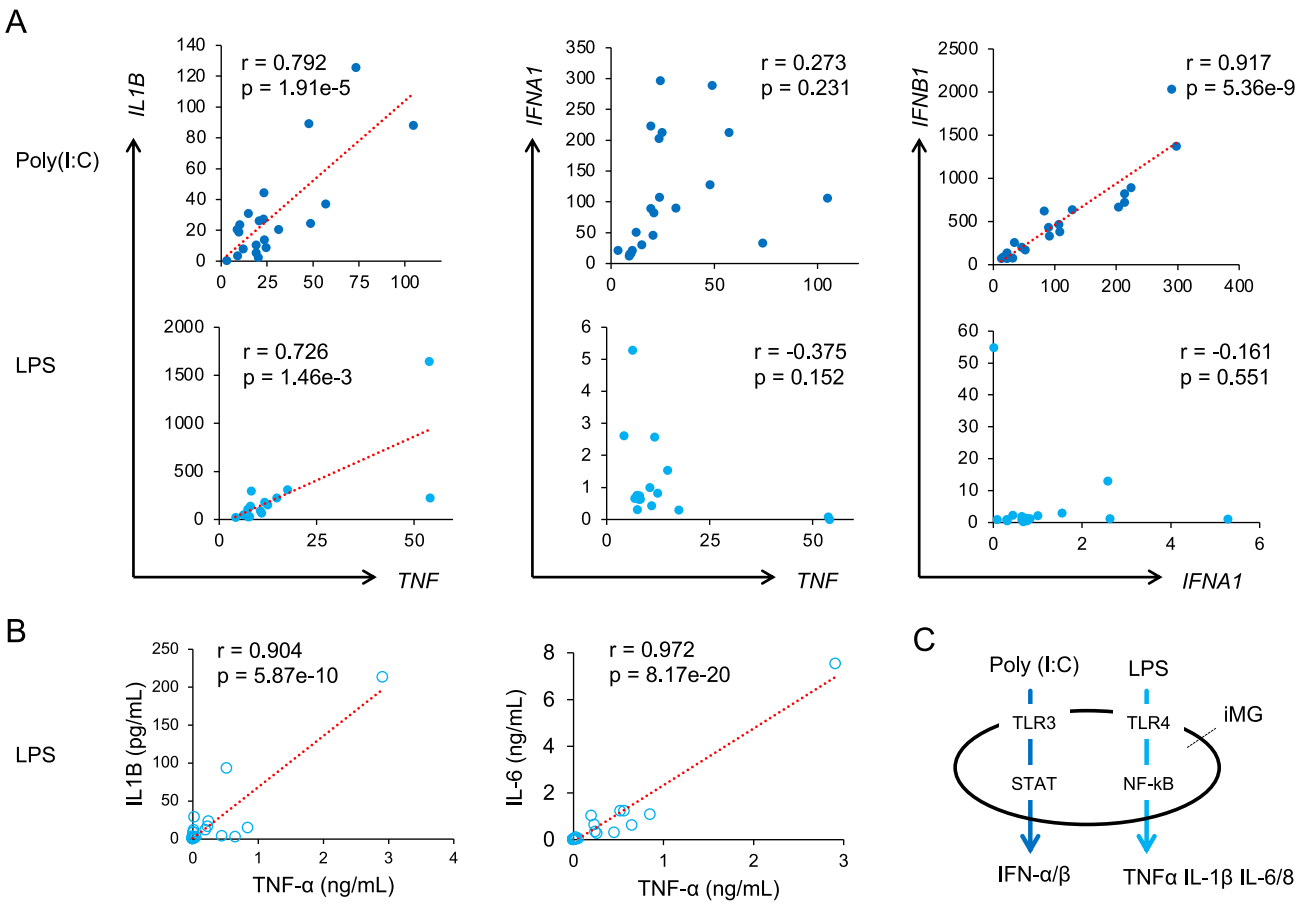

Fig. 3. Activation of distinctive molecular pathways by Poly-I:C and LPS in iMG cells

(A) The correlated expression of NF-κB-dependent genes (*IL1B* and *TNF*) and of type I interferon-coding genes (*IFNA1* and *IFNB1*). No correlation was observed among the genes in different groups. Scatter plots for the expression profiles of the indicated genes after treatment with poly-I:C (n = 21) and LPS (n = 16). R and *P* values represent Pearson's correlation coefficients.

(B) The correlation of IL-1β, TNFα, and IL-6 levels in culture media after LPS treatment. R and P values are shown for the linear regression (n = 31, Pearson's correlation coefficients).

(C) Schematic presentation of the two distinctive pathways in an iMG cell. Poly-I:C and LPS differentially activated their downstream targets, STAT and NF-κB, respectively. These two pathways led to the production of type I interferons (IFN-α/β) and NF-κB-dependent cytokines (TNFα, IL-1β, IL-6 and IL-8).

change after LPS treatment (**Fig. S4**). These data indicated that TNFα was produced in broader subpopulations of iMG than IL-1β. An immunofluorescence analysis verified that strong IL-1β signals were observed in a group of CD14- and ionized calcium-binding adapter molecule 1 (IBA1)-expressing cells (activated iMG) (Fig. 4E).

To investigate the cause-and-effect relationship between the expression of CD14 and production of IL-1β in iMGs, we added atibuclimab, a chimeric monoclonal antibody against CD14 to the culture media 1 h before treatment with LPS. We confirmed that atibuclimab suppressed the populations of iMGs expressing IL-1β (10.4 ± 1.4% to 3.2 ± 1.1%) and TNFα-expressing cells (51.2 ± 15.9% to 28.3 ± 10.5%) after LPS treatment (p = 0.00528 and p = 0.0051, respectively, paired *t*-test; Fig. 5).

3.6. Mitochondrial responses in iMG

To understand the molecular pathways that mediate innate immune responses of iMG, we focused on the mitochondrial stresses experienced after treatment with poly-I:C and LPS. To this end, we analyzed the stability of the mitochondrial inner membrane potential (ΔΨm) using the fluorescent probe JC-1 [37]. We used CCCP as a positive control for decoupling of mitochondrial oxidative phosphorylation (Fig. 6A) [35]. We confirmed that CCCP abolished $\Delta\Psi_m$, showing a decrease to <1% of the control value in the polymer-to-monomer ratio; however, poly-I:C (n = 4) and LPS (n = 3) only partially destabilized $\Delta\Psi_m$ (p = 0.492, Kruskal-Wallis' test; Fig. 6B). Nonetheless, these treatments induced significantly higher rates of Annexin-V+ iMG than at the resting condition (21.0–44.2% *vs.* 13.5–14.0%; $p = 9.09 \times 10^{-3}$, Wilcoxon's rank sum test; Fig. 6C). We therefore investigated whether innate immune ligands induced iMG to produce mitochondrial ROS. We found that these ligands induced 1.05- to 1.29-fold higher amounts of ROS in iMG than in untreated iMG (p = 0.0256, Wilcoxon's rank sum test; Fig. 6D).

An immunofluorescence analysis showed that CX3CR1, PKM2, and IBA1 were co-expressed in LPS-treated iMG (Fig. 6E). Counter-immunofluorescence data further supported the notion that PKM2 signals were observed in iMG expressing the mitochondrial chaperonin, HSP60 (Fig. 6F) [48]. Western blotting showed that the expression of HSP60 was increased after LPS and poly-I:C treatment (Fig. 6G). Compared to the induction of HSP60, PKM2 showed only a subtle increase after treatment. Thus, the expression of PKM2 was considered to be increased only in a small population of iMG under mitochondrial stress with an LPS-induced inflammatory condition.

Because PKM1 and PKM2 are the two end-products of alternative splicing from the *PKM* gene [9], we determined whether iMG from patients with NIDs showed the aberrant expression of these splicing isoforms. The relative expression of PKM2 to PKM1 was significantly increased after treatment with poly-I:C and LPS ($p = 5.52 \times 10^{-3}$, Friedman's test; Fig. 6H). However, iMG from patients with NIDs (n =

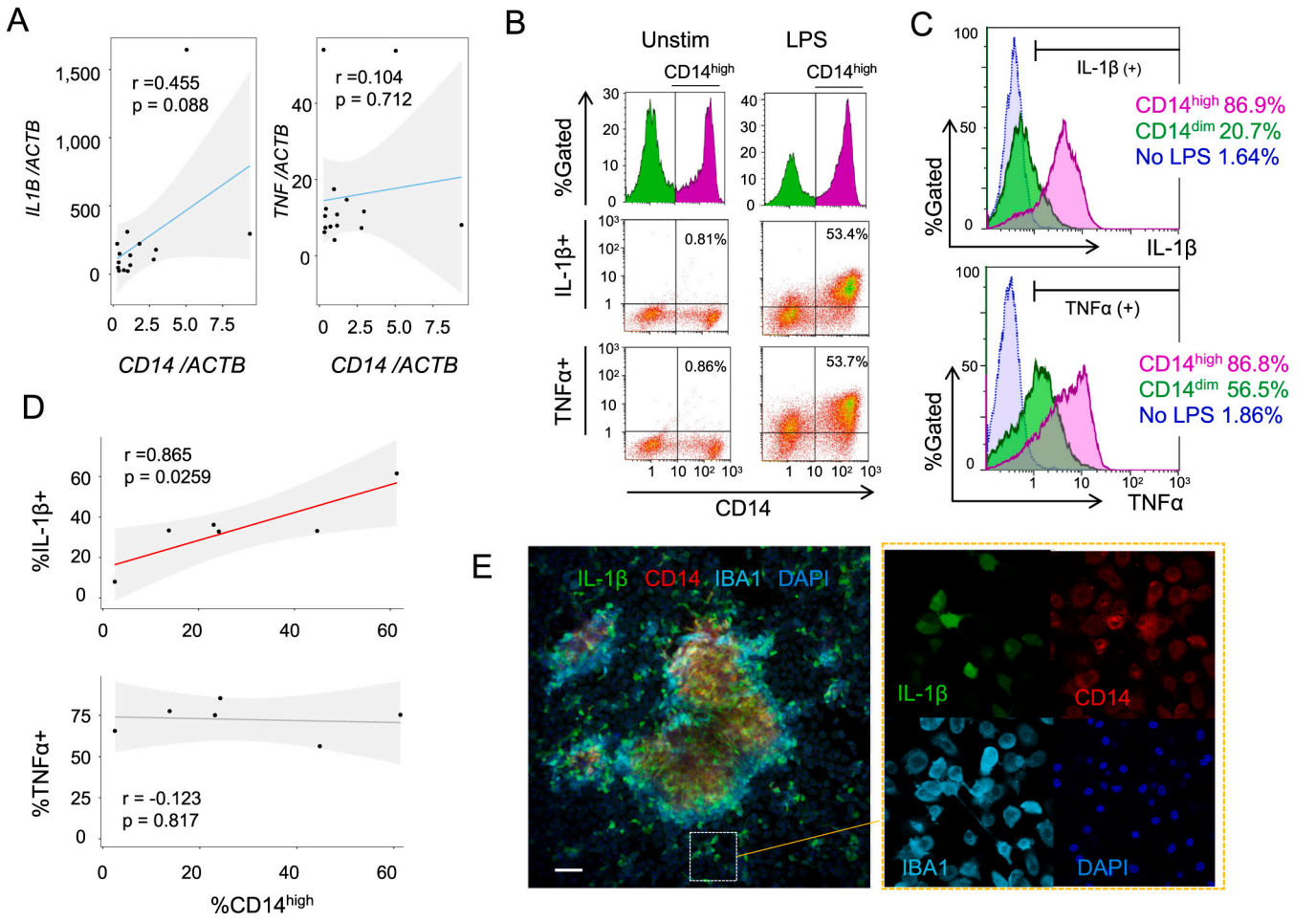

Fig. 4. Heterogeneity in the CD14^{high} cell population and the immunoreactivity of iMG cells
(A) Scatter plots for the expression of *IL1B* and *TNF* (Y-axis) *vs. CD14* (X-axis) in iMG (n = 15) after treatment with LPS for 24 h. For panels A and D, the R and P values indicate Pearson's correlation coefficients. *ACTB* represents the internal standard for qPCR.
(B) Flow cytometry for CD14, IL-1β, and TNFα before and after LPS treatment (3 h). iMG from a healthy adult (HC39) were used for this analysis (B, C). Note that both IL-1β- and TNFα-expressing cells (upper-right quadrant) were increased in number after treatment.
(C) Histograms (% gated cells) show the IL-1β- and TNFα-expressing cells in CD14^{high} (magenta) and CD14^{dim} (green) populations. IL-1β and TNFα were expressed predominantly in the CD14^{high} population after treatment.
(D) The correlations in proportions of IL-1β- and TNFα-positive (+) cells with the CD14^{high} population in iMG from different individuals (n = 6).
(E) An immunofluorescence analysis after LPS treatment (24 h) for iMG #AE-PT15. Scale bar, 100 μm.

10) showed no marked difference in the expression ratio of PKM2 to PKM1, similar to those from controls (n = 5), in either the resting condition or after treatment with poly-I:C and LPS (**Fig. S5**). These results indicated that iMG overexpressed PKM2 under hyperinflammatory conditions.

3.7. *Protective role of PKM2 against hyperinflammation in CD14^{high}-iMG cells*

The experimental data above prompted us to determine whether PKM2 plays a protective role in iMG from exacerbation of the hyperinflammatory condition after the poly-I:C and LPS treatments. We therefore treated iMG with LPS in the presence or absence of the PKM2 allosteric activator DASA-58 [4,51]. When we measured IL-1β concentrations in culture media, DASA-58 appeared to prevent the production of IL-1β after LPS treatment, but the difference did not reach statistical significance with the available samples (n = 4 in each condition, p = 0.500; Wilcoxon's signed-rank test; Fig. 7A). Flow cytometry showed that DASA-58 prominently decreased the rate of IL-1β + cells (61.5% to 27.0%) after LPS treatment (Fig. 7B, left). DASA-58 also had a moderate effect on decreasing the rate of TNFα+ cells (75.4% to 56.5%; Fig. 7B, right). Consistent results were obtained with iMG from other healthy adults (n = 6, Fig. 7C, Table 1).

The differential effect of DASA-58 on IL-1β and TNFα expression appeared to reflect partially overlapping but slightly different subpopulations of iMG expressing these two cytokines after LPS treatment (Fig. 3A). We therefore inspected the results more rigorously by separating the subpopulations of iMG according to their expression of CD14. In agreement with the previous results (Fig. 7A-C), DASA-58 decreased the rate of IL-1β-positive cells in the CD14^{high} subpopulation (86.9% to 41.3%), whereas only a minor effect was observed in the CD14^{dim} subpopulation (21.1% to 7.8%; Fig. 7D). In contrast, DASA-58 only mildly suppressed the rates of TNFα+ iMG in both the CD14^{high} (86.9% to 74.2%) and CD14^{dim} cells (57.1% to 32.8%) subpopulations (Fig. 7D). We attempted to confirm the inhibitory effect of DASA-58 on nuclear translocation of PKM2 after LPS treatment. However, we could not obtain such evidence because of highly heterogenous response of iMGs to LPS (**Fig. S6A—C**).

Finally, we verified these results *via* Western blotting for iMG from two healthy adults (HC38 and HC39) (Table 1). As a reference of cells more homogenously expressing CD14 than iMG, we used the human monocytic leukemia cell line THP-1 [38]. Flow cytometry revealed that

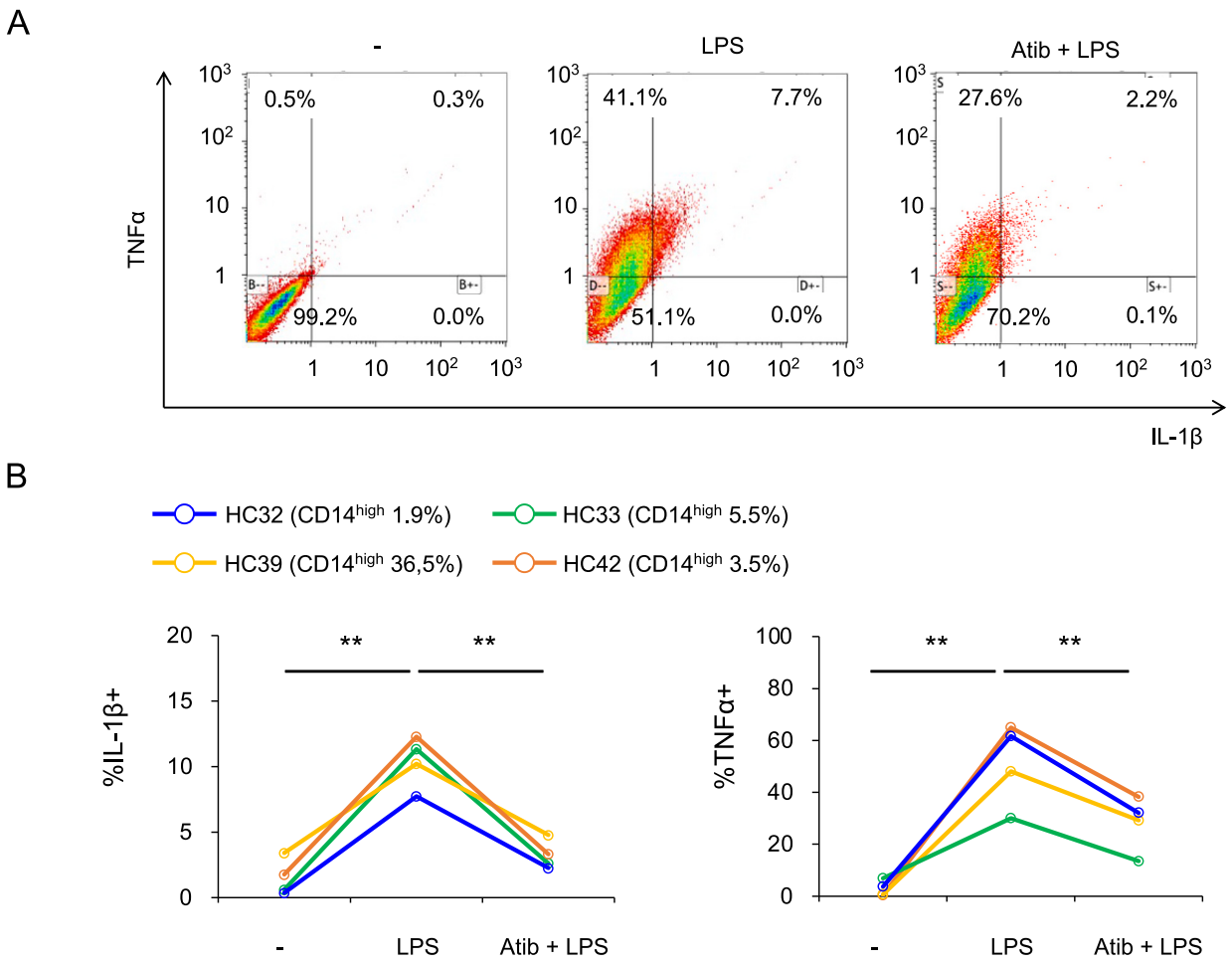

Fig. 5. Atibuclimab attenuates the IL-1β and TNFα production in iMGs after treatment with LPS.
(A) Representative flow cytometry data for iMGs from a healthy adult (HC32). Treatments are shown at the top of each panel: No treatment (−) and LPS with or without the atibuclimab (Atib) pretreatment.
(B) Inhibitory effect of atibuclimab on the LPS-induced IL-1β and TNFα production in iMGs. Sources of iMGs are shown at the top (4 healthy adults). **p < 0.01 (paired *t*-test, $n = 4$ each group).

the majority (99.6%) of THP-1 cells were $CD14^{dim}$ cells (Fig. 7E, upper). Unexpectedly, however, LPS treatment efficiently induced IL-1β (53.7%) and TNFα (70.5%) expression in THP-1 cells (Fig. 7E, lower). Pretreatment with DASA-58 partially prevented THP-1 cells from expressing IL-1β after LPS treatment (36.0%, Fig. 7E, lower left). However, no substantial effect of DASA-58 was observed on the expression of TNFα after LPS treatment (Fig. 7E, lower right). Western blotting did not detect a favorable effect of DASA-58 on decreasing the pro-IL-1β expression after LPS treatment for THP-1, but it efficiently prevented the increase in the STAT1 expression after treatment with poly-I:C and LPS (Fig. 7F, left "THP1").

Because iMG from HC39 (iMG39) harbored $CD14^{high}$ cells at a higher rate (61.4%) than those from HC38 (13.8%; iMG38), pro-IL-1β was more evidently induced in iMG39 than in iMG38 after LPS treatment (middle and right panels, Fig. 7F). Furthermore, DASA-58 explicitly attenuated the pro-IL-1β expression after LPS treatment in iMG39 ("LPS" on the right, Fig. 7F). In contrast, only a negligible effect of DASA-58 on reducing the pro-IL-1β expression was observed in iMG38 ("LPS" in the middle, Fig. 7F). STAT1 was also prominently expressed in iMG39, but not in iMG38 cells after polyI:C and LPS treatment. Again, DASA-58 clearly attenuated the induction of STAT1 in iMG39 ("Mock" *vs.* "D58" on the right, Fig. 7F).

Taken together, our experimental data indicate that iMG from different individuals showed variable proportions of $CD14^{high}$ cells, which largely contributed to the production of IL-1β in response to LPS (Fig. 8). Unknown factors and multiple dimensions in molecular pathways were considered to be responsible for the heterogeneity and divergence of iMG cells with regard to the production of other cytokines, such as TNFα and type I interferons.

4. Discussion

This study provides the first experimental evidence that human iMG from peripheral monocytes show heterogeneous cell populations and differential responses to the innate immune ligands poly-I:C and LPS. Based on the flow cytometry data, we defined subpopulations of iMG as $CD14^{high}$ and $CD14^{dim}$ groups. The expression of IL-1β after LPS treatment was correlated with the population ratio of $CD14^{high}$ to $CD14^{dim}$ cells. Thus, our data recapitulated previous findings that CD14 organizes the LPS-induced inflammatory signaling in human microglia [14]. These data also suggested that "heterogeneity" might be a prerequisite for "divergence" in immunoreactivity of iMG from different individuals [17,33]. The expression of TNFα after LPS treatment did not depend on the presence of $CD14^{high}$ cells, indicating the presence of still-unresolved complexities in both the heterogeneity and diversity of human iMG.

Biochemical data showed that poly-I:C and LPS differentially activated downstream molecular pathways and the expression of pro-inflammatory cytokines in iMG. Specifically, poly-I:C induced the expression of type-I interferons, while LPS did so for TNF-α and IL-1β. Although the concept of heterogeneity in cell populations may

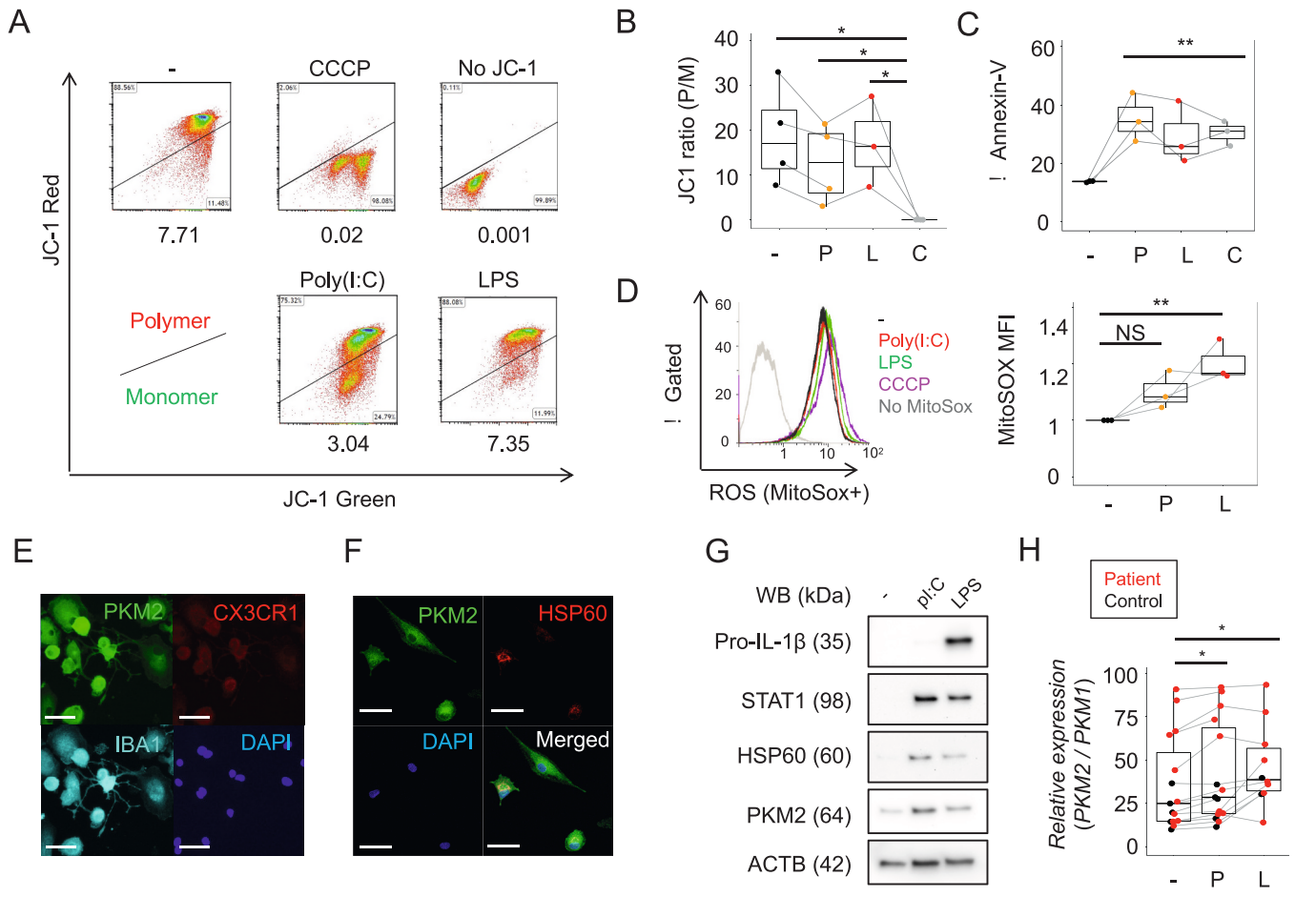

Fig. 6. Mitochondrial instability after treatment with innate immune ligands

(A) A flow cytometry analysis with JC-1 for the mitochondrial inner membrane potential ($\Delta\Psi_m$). The index obtained from the relative ratio of polarized (polymer, red) to depolarized (monomer, green) cells is shown at the bottom of each panel. -, no treatment (A-H).

(B) Box-dot plots for $\Delta\Psi_m$ of iMG before (−) and after treatment with poly-I:C (P), LPS (L) and CCCP (C). Data for iMG from different individuals (n = 3 [LPS] or 4 [other conditions]). *P < 0.05 (Kruskal-Wallis' test).

(C) Box-dot plots for Annexin-V-positive cells in iMG before and after the indicated treatments. Data for iMG from different individuals (n = 3). **$P < 0.01$ (Wilcoxon's rank sum test).

(D) Histograms (% gated cells) for mitoSox+ cells before and after the indicated treatments. Box-dot plots in the right panel show data with 3 iMG from different individuals. NS, not significant. **P < 0.01 (Wilcoxon's rank sum test).

(E, F) Immunofluorescence studies for iMG #AE-PT15 (E) and HC39 (F). Note that PKM2 was co-expressed in iMG with IBA1, CX3CR1, and HSP60. Scale bar, 50 μm.

(G) Representative Western blotting for iMG from HC39. Note that the expression of HSP60 and PKM2 was increased after treatment with poly-I:C and LPS.

(H) Box-line plots show the relative expression ratio of PKM2/PKM1 in iMG from each participant before (−) and after the indicated treatments with poly-I:C (P) and LPS (L) for 24 h. *$p < 0.05$ (n = 15 before and after poly-I:C, $n = 10$ after LPS; Wilcoxon's signed-rank test). Red and black dots represent patients and controls, respectively.

reasonably explain this result, we cannot conclude that distinct or overlapping subgroups of iMG responded to these ligands. Bulk-prepared samples were unable to identify a group of iMG that might react with both poly-I:C and LPS or those showing a higher reactivity to one ligand than to another. It therefore might be worth investigating the transcriptomic profile of iMG at a single-cell resolution before and after stimulation with these ligands [17,33,41].

We found that mitochondrial responses were also heterogeneous among iMG after treatment with poly-I:C and LPS. Because of the small-scale procedure of blood sampling, we were unable to assess the association of decreased ΔΨm with the population ratio of $CD14^{high}$ cells among iMG cells from the same individual in this study. However, immunofluorescence data indicated that HSP60 and PKM2 were co-expressed in activated iMG cells after LPS treatment. Consistently, several reports have shown that an impaired mitochondrial function augments the inflammasome-driven proinflammatory cascade in microglia [12]. Such bidirectional interplays between mitochondria and inflammation cascades have been considered essential for the development of NIDs and neurodegeneration [29]. Thus, we might be able to rationalize that the magnitude of mitochondrial stress and dysfunction represents the variable degree of inflammation in each iMG cell. Based on these findings, we speculate that mitochondria regulate heterogeneous and divergent inflammatory responses of microglia in the human brain exposed to various immune ligands [6].

PKM2 is a rate-limiting enzyme of glycolysis and metabolic reprogramming in malignant tissues, called Warburg's effect [62]. In addition to the crucial role of PKM2 in tumorigenesis [63], the pharmaceutical activation of PKM2 has been shown to exert beneficial effects on controlling the inflammatory responses in microglia and macrophages [4,52]. Activators of PKM2 induces conformational change of the protein, promoting the formation of a homo-tetramer, the most active form of the enzyme. Activated PKM2 then attaches to mitochondrial outer membrane and plays a regulatory role in various immune cells against inflammatory processes. This is known as an opposing function of the dimeric PKM2, which acts as a coactivator of proinflammatory molecules, signal transducer and activator of transcription 3 (STAT3) and

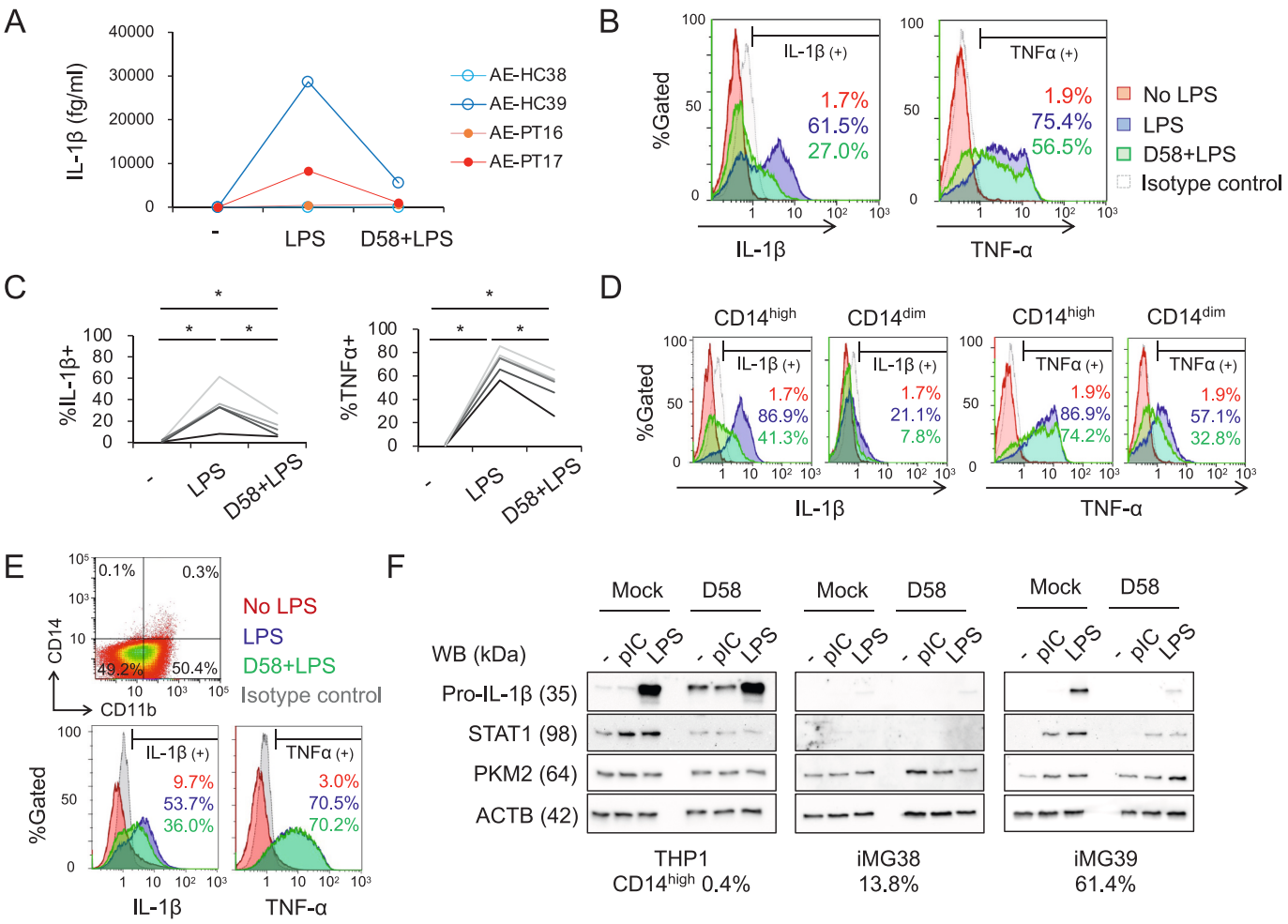

Fig. 7. Regulatory roles of pyruvate kinase M2 in the immunoreactivity of iMG cells

(A) Variable IL-1β concentrations in culture media before (−) and after LPS treatment of iMG for 24 h (n = 4). The differential effects of LPS in the presence or absence of DASA-58 are shown in the line-connected plots. D58, DASA-58; −, unstimulated.

(B) Histograms (% gated cells) show the difference in the population of IL-1β- and TNFα-expressing cells before (red) and after (blue) LPS treatment (3 h) determined by flow cytometry. The effects of pretreatment with DASA-58 are shown in green. For panels B and D, flow cytometry data were obtained from iMG39.

(C) Inhibitory effects of DASA-58 (D58) on the immunoreactivity of iMG from different individuals (n = 6). The frequencies (%) of IL-1β- and TNFα-expressing cells before and after LPS treatment are shown in the line plots. *$p < 0.05$ (Wilcoxon's signed-rank test).

(D) Differential effects of DASA-58 on IL-1β and TNFα expressions in $CD14^{high}$ and $CD14^{dim}$ iMG. Cell counts in panel B were separated into the $CD14^{high}$ and $CD14^{dim}$ subpopulations.

(E) Flow cytometry data for THP-1. The surface expression of CD11b and CD14 (upper) and the intracellular expression of IL-1β (lower left) and TNFα (lower right) are shown with color histograms (% gated cells): No LPS (red), LPS with (green) and without DASA-58 pretreatment (blue).

(F) Western blotting for THP-1 (left), iMG38 (middle), and iMG39 (right). Populations of $CD14^{high}$ cells are shown at the bottom. Note that pro-IL-1β was highly expressed in THP-1 and iMG39 after LPS treatment for 24 h, and that DASA-58 most effectively decreased the expression of IL-1β in iMG39.

hypoxia-inducible factor 1 alpha (HIF-1α) [30,52,62]. Our data did not support evidence for the inhibitory effect of DASA-58 on nuclear translocation of PKM2 after LPS treatment. However, we confirmed that pretreatment of iMG with DASA-58 decreased the production of IL-1β and TNFα after LPS treatment. Heterogeneity in immune responses of iMGs to LPS might explain this discrepancy. The favorable effect of DASA-58 suggested that PKM2 and mitochondria might be potential targets of molecular intervention for the broad category of NIDs [10,11,60]. Alternatively, preconditioning with DASA-58 may expand the therapeutic potential of iMG and stem cells in future translational research [34,49].

Childhood-onset NIDs in this study included a wide variety of clinical diagnoses, including ADS [5], AESD [56], and other forms of encephalitis with or without known pathogens [36]. Because each diagnostic category represents a heterogeneous group of diseases, we can hardly hypothesize the convergent mechanisms among divergent phenotypes of NIDs. It is therefore likely that microglia contribute differently to the development of each NID, either in a pro- or anti-inflammatory direction [21]. Activation of PKM2 was also shown to prevent iMG cells from producing IL-1β and STAT1. Thus, the microglia in these patients might contain a subset of mitochondria that are highly reactive to immune ligands in environments. In agreement with this concept, the number of activated microglia was increased in surgically resected tissues from children with AESD [15] and in the brains of animal models for post-status epilepticus encephalopathy [47]. Clarifying the molecular pathways specifically activated in each category of NIDs might help us understand how heterogeneous subtypes of microglia contribute to the development of or protection against disease.

Several limitations must be considered before conclusion. First, we focused only on selected molecules in flow cytometry and immunofluorescence in order to clarify the heterogeneity and diversity of iMG cells. More comprehensive methods, such as flow-mass spectrometry, will disclose a broader landscape of phenotypic heterogeneity of iMG from individuals with different clinical backgrounds. Phenotypic divergence

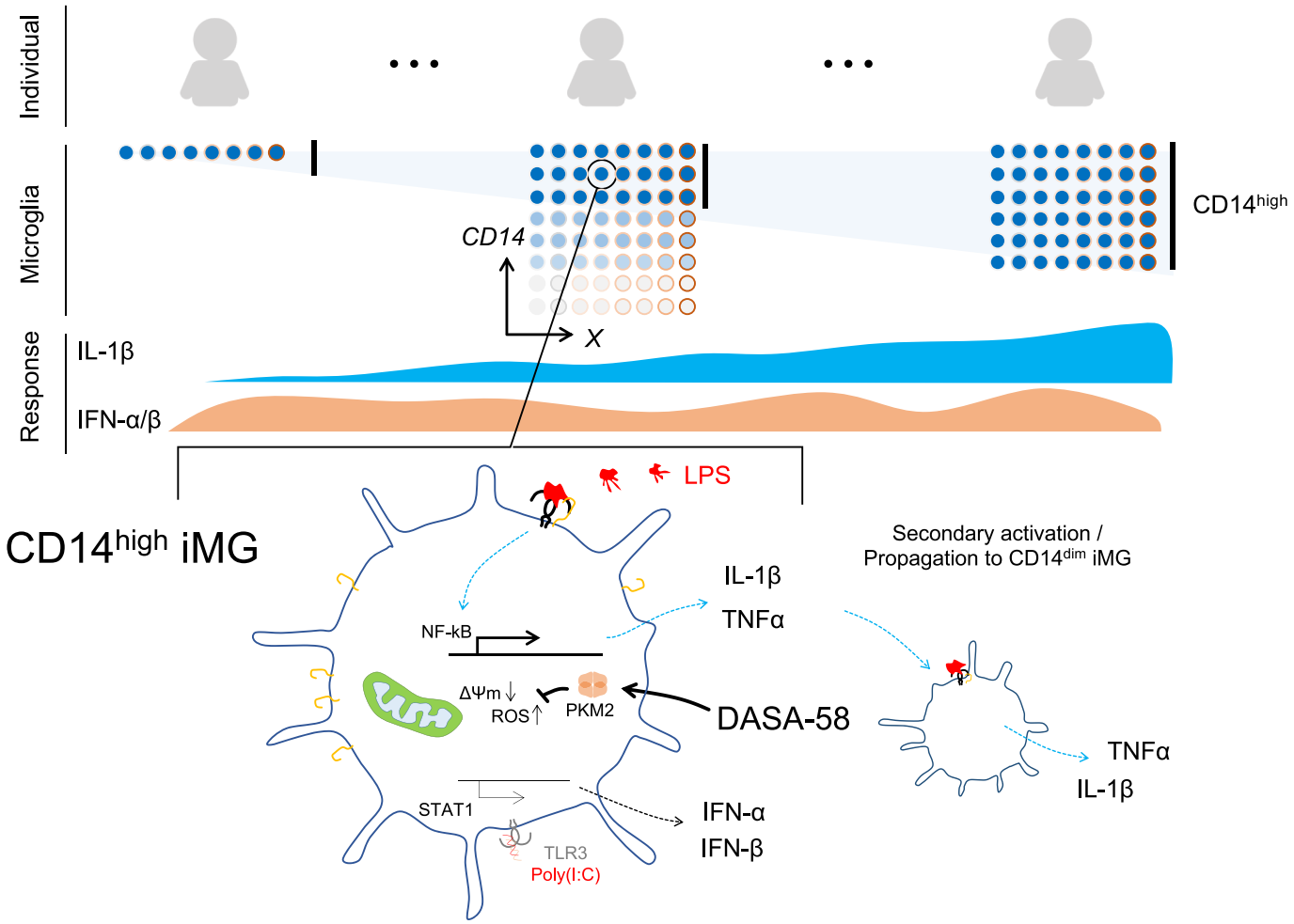

Fig. 8. A schematic model for the heterogeneity and divergent immunoreactivity of iMG cells.
Human microglia and iMG in each individual are likely to consist of variable proportions of $CD14^{high}$ cells (deep blue). In this study, we first demonstrated that LPS induced IL-1β proportionate to the $CD14^{high}$ population ratio (blue gradient and slope). As-yet-unidentified factors (X, salmon gradient) may regulate the expression of TNFα and type I interferons (IFN-α and IFN-β) in different subsets of iMG. In a $CD14^{high}$-iMG cell (lower panel), LPS activates the NF-κB-dependent transcription, while poly-I:C triggers the STAT1-dependent gene expression. The PKM2 activator DASA-58 protects the inflammatory response to LPS in $CD14^{high}$ iMG. The CD14-dependent release of IL-1β and TNFα may extend to $CD14^{dim}$ iMG as secondary activation of cytokine production. (For interpretation of the references to color in this figure legend, the reader is referred to the web version of this article.)

might not be restricted to the cytokine production in iMGs from different individuals. Cell motility and migration assays are necessary for further characterization of iMGs. Second, no cytokine-encoding genes were found to be overly expressed in iMG from children with NIDs because we performed qPCR only from bulk-prepared mRNA. Single-cell RNA sequencing may help identify which genes are uniquely upregulated and how many of iMG express particular subsets of genes in response to innate immune ligands. This modality will provide much deeper information than the current dataset about heterogeneity of iMGs in terms of specific cell populations and molecular pathways activated by the innate immune ligands. Third, we analyzed only a small number of iMG cells from currently available patients in each disease category of NIDs. The number of samples was too small to interpret our data as representative of all patients. It was also hard to characterize innate immune responses of iMGs from pediatric patients without sufficient number of samples from healthy children. In compliance with the ethics statement, we have obtained written informed consent from parents of the pediatric patients before sampling. Thus, we could not collect blood samples from healthy children for the purpose of this study, but established control iMGs only from two children, who had epilepsy (AE-CT3 and AE-CT4). Because homeostatic markers of microglia are currently known to decline with aging [20], we cannot exclude the possibility that immunoreactivity of iMGs might differ with the age of subjects. By accumulating single-cell transcriptomic data, we might detect a certain type of heterogeneity in the expression profiles for each NID.

In conclusion, we found that human iMG show diverse reactivity to poly-I:C and LPS according to the population of $CD14^{high}$ cells. The functional role of PKM2 linked the heterogeneous cell population and diverse immunoreactivity of iMG to these ligands. Our data indicate that human iMG can help clarify the pathogenic mechanisms underlying various NIDs in childhood. These efforts provide promising insight into therapeutic targets for future translational medicine for affected children.

CRediT authorship contribution statement

Yonemoto K: Conceptualization; Formal analysis; Writing – original draft; Writing – review and editing. **Fujii F:** Data curation; Supervision; Writing – review and editing. **Taira R:** Data curation; Supervision; Writing – review and editing. **Ohgidani M:** Data curation; Supervision; Writing – review and editing. **Eguchi:** Investigation; Resources. **Okuzono:** Investigation; Resources. **Ichimiya:** Investigation; Resources. **Sonoda:** Investigation; Resources. **Chong:** Investigation; Resources. **Goto:** Investigation; Resources. **Kanemasa H:** Investigation; Resources.

Motomura Y: Investigation; Resources. **Ishimura M:** Investigation; Resources. **Koga Y:** Investigation; Resources. **Tsujimura K:** Investigation; Resources; Supervision; Methodology. **Hashiguchi T:** Resources; Supervision; Methodology. **Torisu H:** Resources; Supervision; Funding acquisition. **Kira R:** Resources; Supervision; Funding acquisition. **Kato TA:** Resources; Supervision; Funding acquisition. **Sakai Y:** Conceptualization; Formal analysis; Supervision; Data curation; Funding acquisition; Writing – original draft; Writing – review and editing. **Ohga S:** Conceptualization; Supervision; Data curation; Funding acquisition; and Writing – review and editing.

Funding

This study was supported by JSPS KAKENHI grant numbers JP21K07865 (Okuzono), JP 18K15677, JP22K07893 (Sonoda), JP23K07334 (Sakai); AMED under the grant number JP20ek0109411, JP20wm0325002h; a research grant for prion diseases from the Ministry of Health, Labour and Welfare of Japan (JP23FC0201 and JP21FC1005); Japan Epilepsy Research Foundation, and Kawano Masanori Memorial Public Interest Incorporated Foundation for Promotion of Pediatrics (Sakai).

Declaration of Competing Interest

None.

Data availability

The data that support the findings of this study are available in the methods and supplemental information of this article.

Acknowledgments

We thank Professor Toshiro Hara (President, Fukuoka Children's Hospital), Professor Shigenobu Kanba (Kyushu University), Professor Kazuaki Nonaka (Kyushu University), and Dr. Hisanori Nishio (Kyushu University, deceased) for their essential advice; we also thank Dr. Tamami Tanaka and Ms. Ryoko Unose for assisting with flow cytometry.

Appendix A. Supplementary data

Supplementary data to this article can be found online at https://doi.org/10.1016/j.clim.2023.109756.

References

[1] S. Akamine, S. Okuzono, H. Yamamoto, D. Setoyama, N. Sagata, M. Ohgidani, T. A. Kato, T. Ishitani, H. Kato, K. Masuda, Y. Matsushita, H. Ono, Y. Ishizaki, M. Sanefuji, H. Saitsu, N. Matsumoto, D. Kang, S. Kanba, Y. Nakabeppu, Y. Sakai, S. Ohga, GNAO1 organizes the cytoskeletal remodeling and firing of developing neurons, FASEB J. 34 (2020) 16601–16621.
[2] S. Alotaibi, J. Kennedy, R. Tellier, D. Stephens, B. Banwell, Epstein-Barr virus in pediatric multiple sclerosis, JAMA 291 (2004) 1875–1879.
[3] M. Andoh, R. Koyama, Microglia regulate synaptic development and plasticity, Dev. Neurobiol. 81 (2021) 568–590.
[4] S. Angiari, M.C. Runtsch, C.E. Sutton, E.M. Palsson-McDermott, B. Kelly, N. Rana, H. Kane, G. Papadopoulou, E.L. Pearce, K.H.G. Mills, L.A.J. O'Neill, Pharmacological activation of pyruvate kinase M2 inhibits CD4(+) T cell pathogenicity and suppresses autoimmunity, Cell Metab. 31 (391–405) (2020), e398.
[5] T. Armangue, G. Olive-Cirera, E. Martinez-Hernandez, M. Sepulveda, R. Ruiz-Garcia, M. Munoz-Batista, H. Arino, V. Gonzalez-Alvarez, A. Felipe-Rucian, M. Jesus Martinez-Gonzalez, V. Cantarin-Extremera, M. Concepcion Miranda-Herrero, L. Monge-Galindo, M. Tomas-Vila, E. Miravet, I. Malaga, G. Arrambide, C. Auger, M. Tintore, X. Montalban, A. Vanderver, F. Graus, A. Saiz, J. Dalmau, M. O.G.S.G. Spanish Pediatric anti., Associations of paediatric demyelinating and encephalitic syndromes with myelin oligodendrocyte glycoprotein antibodies: a multicentre observational study, Lancet Neurol. 19 (2020) 234–246.
[6] D. Arnoult, F. Soares, I. Tattoli, S.E. Girardin, Mitochondria in innate immunity, EMBO Rep. 12 (2011) 901–910.
[7] E.S. Beck, D.S. Reich, Multiple sclerosis in 2021: progress against progression, Lancet Neurol. 21 (2022) 12–13.
[8] K. Bjornevik, M. Cortese, B.C. Healy, J. Kuhle, M.J. Mina, Y. Leng, S.J. Elledge, D. W. Niebuhr, A.I. Scher, K.L. Munger, A. Ascherio, Longitudinal analysis reveals high prevalence of Epstein-Barr virus associated with multiple sclerosis, Science 375 (2022) 296–301.
[9] S. Calabretta, P. Bielli, I. Passacantilli, E. Pilozzi, V. Fendrich, G. Capurso, G. D. Fave, C. Sette, Modulation of PKM alternative splicing by PTBP1 promotes gemcitabine resistance in pancreatic cancer cells, Oncogene 35 (2016) 2031–2039.
[10] K.S. Carvalho, Mitochondrial dysfunction in demyelinating diseases, Semin. Pediatr. Neurol. 20 (2013) 194–201.
[11] G. Cenini, W. Voos, Mitochondria as potential targets in Alzheimer Disease therapy: an update, Front. Pharmacol. 10 (2019) 902.
[12] C. Culmsee, S. Michels, S. Scheu, V. Arolt, U. Dannlowski, J. Alferink, Mitochondria, microglia, and the immune system-how are they linked in affective disorders? Front. Psychol. 9 (2018) 739.
[13] Y. Dong, V.W. Yong, When encephalitogenic T cells collaborate with microglia in multiple sclerosis, Nat. Rev. Neurol. 15 (2019) 704–717.
[14] K. Fassbender, S. Walter, S. Kuhl, R. Landmann, K. Ishii, T. Bertsch, A.K. Stalder, F. Muehlhauser, Y. Liu, A.J. Ulmer, S. Rivest, A. Lentschat, E. Gulbins, M. Jucker, M. Staufenbiel, K. Brechtel, J. Walter, G. Multhaup, B. Penke, Y. Adachi, T. Hartmann, K. Beyreuther, The LPS receptor (CD14) links innate immunity with Alzheimer's disease, FASEB J. 18 (2004) 203–205.
[15] Y. Fujita, J.I. Takanashi, H. Takei, S. Ota, K. Fujii, H. Sakuma, M. Hayashi, Activated microglia in acute encephalopathy with biphasic seizures and late reduced diffusion, J. Neurol. Sci. 366 (2016) 91–93.
[16] S. Genth-Zotz, S. von Haehling, A.P. Bolger, P.R. Kalra, R. Wensel, A.J. Coats, H. D. Volk, S.D. Anker, The anti-CD14 antibody IC14 suppresses ex vivo endotoxin stimulated tumor necrosis factor-alpha in patients with chronic heart failure, Eur. J. Heart Fail. 8 (2006) 366–372.
[17] U. Gertig, U.K. Hanisch, Microglial diversity by responses and responders, Front. Cell. Neurosci. 8 (2014) 101.
[18] F. Ginhoux, M. Greter, M. Leboeuf, S. Nandi, P. See, S. Gokhan, M.F. Mehler, S. J. Conway, L.G. Ng, E.R. Stanley, I.M. Samokhvalov, M. Merad, Fate mapping analysis reveals that adult microglia derive from primitive macrophages, Science 330 (2010) 841–845.
[19] T. Goldmann, T. Blank, M. Prinz, Fine-tuning of type I IFN-signaling in microglia–implications for homeostasis, CNS autoimmunity and interferonopathies, Curr. Opin. Neurobiol. 36 (2016) 38–42.
[20] K. Grabert, T. Michoel, M.H. Karavolos, S. Clohisey, J.K. Baillie, M.P. Stevens, T. C. Freeman, K.M. Summers, B.W. McColl, Microglial brain region-dependent diversity and selective regional sensitivities to aging, Nat. Neurosci. 19 (2016) 504–516.
[21] B.L. Guerrero, N.L. Sicotte, Microglia in multiple sclerosis: friend or foe? Front. Immunol. 11 (2020) 374.
[22] A. Hoshino, M. Saitoh, A. Oka, A. Okumura, M. Kubota, Y. Saito, J. Takanashi, S. Hirose, T. Yamagata, H. Yamanouchi, M. Mizuguchi, Epidemiology of acute encephalopathy in Japan, with emphasis on the association of viruses and syndromes, Brain and Development 34 (2012) 337–343.
[23] E. Kamma, W. Lasisi, C. Libner, H.S. Ng, J.R. Plemel, Central nervous system macrophages in progressive multiple sclerosis: relationship to neurodegeneration and therapeutics, J. Neuroinflammation 19 (2022) 45.
[24] T.S. Kapellos, L. Bonaguro, I. Gemund, N. Reusch, A. Saglam, E.R. Hinkley, J. L. Schultze, Human monocyte subsets and phenotypes in major chronic inflammatory diseases, Front. Immunol. 10 (2019) 2035.
[25] H. Kato, T. Thi Mai Pham, H. Yamaza, K. Masuda, Y. Hirofuji, X. Han, H. Sato, T. Taguchi, K. Nonaka, Mitochondria regulate the differentiation of stem cells from human exfoliated deciduous teeth, Cell Struct. Funct. 42 (2017) 105–116.
[26] S. Lee, T. Morioka, P.F. Chong, S.O. Suzuki, T. Imagi, N. Murakami, H. Baba, R. Kira, Subcortical axonal loss with glial reactions following partial status epilepticus with neuroradiological findings of reduced subcortical diffusion, Neurol. Sci. 40 (2019) 851–855.
[27] Q. Li, B.A. Barres, Microglia and macrophages in brain homeostasis and disease, Nat. Rev. Immunol. 18 (2018) 225–242.
[28] Y. Li, L. Yin, Z. Fan, B. Su, Y. Chen, Y. Ma, Y. Zhong, W. Hou, Z. Fang, X. Zhang, Microglia: a potential therapeutic target for Sepsis-associated encephalopathy and Sepsis-associated chronic pain, Front. Pharmacol. 11 (2020), 600421.
[29] M.M. Lin, N. Liu, Z.H. Qin, Y. Wang, Mitochondrial-derived damage-associated molecular patterns amplify neuroinflammation in neurodegenerative diseases, Acta Pharmacol. Sin. 0 (2022) 1–9.
[30] W. Luo, H. Hu, R. Chang, J. Zhong, M. Knabel, R. O'Meally, R.N. Cole, A. Pandey, G.L. Semenza, Pyruvate kinase M2 is a PHD3-stimulated coactivator for hypoxia-inducible factor 1, Cell 145 (2011) 732–744.
[31] A. Mangalam, S.K. Shahi, D. Luckey, M. Karau, E. Marietta, N. Luo, R.S. Choung, J. Ju, R. Sompallae, K. Gibson-Corley, R. Patel, M. Rodriguez, C. David, V. Taneja, J. Murray, Human gut-derived commensal Bacteria suppress CNS inflammatory and Demyelinating Disease, Cell Rep. 20 (2017) 1269–1277.
[32] T. Masuda, R. Sankowski, O. Staszewski, C. Bottcher, L. Amann, C. Sagar, S. Scheiwe, P. Nessler, G. van Kunz, V.A. Loo, P.C. Coenen, A. Reinacher, U. Michel, R. Sure, D. Gold, J. Grun, C. Stadelmann Priller, M. Prinz, Author correction: spatial and temporal heterogeneity of mouse and human microglia at single-cell resolution, Nature 568 (2019) E4.
[33] T. Masuda, R. Sankowski, O. Staszewski, M. Prinz, Microglia heterogeneity in the single-cell era, Cell Rep. 30 (2020) 1271–1281.
[34] L. Mazzini, M. Gelati, D.C. Profico, G. Sgaravizzi, M. Projetti Pensi, G. Muzi, C. Ricciolini, L. Rota Nodari, S. Carletti, C. Giorgi, C. Spera, F. Domenico, E. Bersano, F. Petruzzelli, C. Cisari, A. Maglione, M.F. Sarnelli, A. Stecco, G. Querin, S. Masiero, R. Cantello, D. Ferrari, C. Zalfa, E. Binda, A. Visioli,

D. Trombetta, A. Novelli, B. Torres, L. Bernardini, A. Carriero, P. Prandi, S. Servo, A. Cerino, V. Cima, A. Gaiani, N. Nasuelli, M. Massara, J. Glass, G. Soraru, N. M. Boulis, A.L. Vescovi, Human neural stem cell transplantation in ALS: initial results from a phase I trial, J. Transl. Med. 13 (2015) 17.
[35] T.G. McWilliams, A.R. Prescott, L. Montava-Garriga, G. Ball, F. Singh, E. Barini, M. M.K. Muqit, S.P. Brooks, I.G. Ganley, Basal Mitophagy occurs independently of PINK1 in mouse tissues of high metabolic demand, Cell Metab. 27 (439–449) (2018), e435.
[36] M. Mizuguchi, T. Ichiyama, G. Imataka, A. Okumura, T. Goto, H. Sakuma, J. I. Takanashi, K. Murayama, T. Yamagata, H. Yamanouchi, T. Fukuda, Y. Maegaki, Guidelines for the diagnosis and treatment of acute encephalopathy in childhood, Brain and Development 43 (2021) 2–31.
[37] S. Mizuguchi, K. Gotoh, Y. Nakashima, D. Setoyama, Y. Takata, S. Ohga, D. Kang, Mitochondrial reactive oxygen species are essential for the development of psoriatic inflammation, Front. Immunol. 12 (2021), 714897.
[38] C.M. Mulvey, L.M. Breckels, O.M. Crook, D.J. Sanders, A.L.R. Ribeiro, A. Geladaki, A. Christoforou, N.K. Britovsek, T. Hurrell, M.J. Deery, L. Gatto, A.M. Smith, K. S. Lilley, Spatiotemporal proteomic profiling of the pro-inflammatory response to lipopolysaccharide in the THP-1 human leukaemia cell line, Nat. Commun. 12 (2021) 5773.
[39] M. Ohgidani, T.A. Kato, S. Kanba, Introducing directly induced microglia-like (iMG) cells from fresh human monocytes: a novel translational research tool for psychiatric disorders, Front. Cell. Neurosci. 9 (2015) 184.
[40] M. Ohgidani, T.A. Kato, D. Setoyama, N. Sagata, R. Hashimoto, K. Shigenobu, T. Yoshida, K. Hayakawa, N. Shimokawa, D. Miura, H. Utsumi, S. Kanba, Direct induction of ramified microglia-like cells from human monocytes: dynamic microglial dysfunction in Nasu-Hakola disease, Sci. Rep. 4 (2014) 4957.
[41] M. Olah, V. Menon, N. Habib, M.F. Taga, Y. Ma, C.J. Yung, M. Cimpean, A. Khairallah, G. Coronas-Samano, R. Sankowski, D. Grun, A.A. Kroshilina, D. Dionne, R.A. Sarkis, G.R. Cosgrove, J. Helgager, J.A. Golden, P.B. Pennell, M. Prinz, J.P.G. Vonsattel, A.F. Teich, J.A. Schneider, D.A. Bennett, A. Regev, W. Elyaman, E.M. Bradshaw, P.L. De Jager, Single cell RNA sequencing of human microglia uncovers a subset associated with Alzheimer's disease, Nat. Commun. 11 (2020) 6129.
[42] P.R. Ormel, R. Vieira de Sa, E.J. van Bodegraven, H. Karst, O. Harschnitz, M.A. M. Sneeboer, L.E. Johansen, R.E. van Dijk, N. Scheefhals, A. Berdenis van Berlekom, E. Ribes Martinez, S. Kling, H.D. MacGillavry, L.H. van den Berg, R. S. Kahn, E.M. Hol, L.D. de Witte, R.J. Pasterkamp, Microglia innately develop within cerebral organoids, Nat. Commun. 9 (2018) 4167.
[43] E.M. Palsson-McDermott, A.M. Curtis, G. Goel, M.A. Lauterbach, F.J. Sheedy, L. E. Gleeson, M.W. van den Bosch, S.R. Quinn, R. Domingo-Fernandez, D. G. Johnston, J.K. Jiang, W.J. Israelsen, J. Keane, C. Thomas, C. Clish, M. Vander Heiden, R.J. Xavier, L.A. O'Neill, Pyruvate kinase M2 regulates Hif-1alpha activity and IL-1beta induction and is a critical determinant of the Warburg effect in LPS-activated macrophages, Cell Metab. 21 (2015) 65–80.
[44] R.C. Paolicelli, G. Bolasco, F. Pagani, L. Maggi, M. Scianni, P. Panzanelli, M. Giustetto, T.A. Ferreira, E. Guiducci, L. Dumas, D. Ragozzino, C.T. Gross, Synaptic pruning by microglia is necessary for normal brain development, Science 333 (2011) 1456–1458.
[45] J.R. Plemel, J.A. Stratton, N.J. Michaels, K.S. Rawji, E. Zhang, S. Sinha, C. S. Baaklini, Y. Dong, M. Ho, K. Thorburn, T.N. Friedman, S. Jawad, C. Silva, A. V. Caprariello, V. Hoghooghi, J. Yue, A. Jaffer, K. Lee, B.J. Kerr, R. Midha, P. K. Stys, J. Biernaskie, V.W. Yong, Microglia response following acute demyelination is heterogeneous and limits infiltrating macrophage dispersion, Sci. Adv. 6 (2020) eaay6324.
[46] R.M. Ransohoff, A polarizing question: do M1 and M2 microglia exist? Nat. Neurosci. 19 (2016) 987–991.
[47] F. Sano, E. Shigetomi, Y. Shinozaki, H. Tsuzukiyama, K. Saito, K. Mikoshiba, H. Horiuchi, D.L. Cheung, J. Nabekura, K. Sugita, M. Aihara, S. Koizumi, Reactive astrocyte-driven epileptogenesis is induced by microglia initially activated following status epilepticus, JCI Insight 6 (9) (2021), e135391.
[48] F. Santacatterina, M. Sanchez-Arago, M. Catalan-Garcia, G. Garrabou, C.N. de Arenas, J.M. Grau, F. Cardellach, J.M. Cuezva, Pyruvate kinase M2 and the mitochondrial ATPase inhibitory factor 1 provide novel biomarkers of dermatomyositis: a metabolic link to oncogenesis, J. Transl. Med. 15 (2017) 29.
[49] S. Sarkar, R. Yang, R. Mirzaei, K. Rawji, C. Poon, M.K. Mishra, F.J. Zemp, P. Bose, J. Kelly, J.F. Dunn, V.W. Yong, Control of brain tumor growth by reactivating myeloid cells with niacin, Sci. Transl. Med. 12 (2020) eaay9924.
[50] D.P. Schafer, E.K. Lehrman, A.G. Kautzman, R. Koyama, A.R. Mardinly, R. Yamasaki, R.M. Ransohoff, M.E. Greenberg, B.A. Barres, B. Stevens, Microglia sculpt postnatal neural circuits in an activity and complement-dependent manner, Neuron 74 (2012) 691–705.
[51] S.M. Seki, K. Posyniak, R. McCloud, D.A. Rosen, A. Fernandez-Castaneda, R. M. Beiter, V. Serbulea, S.C. Nanziri, N. Hayes, C. Spivey, L. Gemta, T.N.J. Bullock, K.L. Hsu, A. Gaultier, Modulation of PKM activity affects the differentiation of TH17 cells, Sci. Signal. 13 (2020) eaay9217.
[52] T. Shirai, R.R. Nazarewicz, B.B. Wallis, R.E. Yanes, R. Watanabe, M. Hilhorst, L. Tian, D.G. Harrison, J.C. Giacomini, T.L. Assimes, J.J. Goronzy, C.M. Weyand, The glycolytic enzyme PKM2 bridges metabolic and inflammatory dysfunction in coronary artery disease, J. Exp. Med. 213 (2016) 337–354.
[53] M. Sonoda, M. Ishimura, K. Eguchi, Y. Yada, N. Lenhartova, A. Shiraishi, T. Tanaka, Y. Sakai, S. Ohga, Progressive B cell depletion in human MALT1 deficiency, Clin. Exp. Immunol. 206 (2021) 237–247.
[54] V. Stratoulias, J.L. Venero, M.E. Tremblay, B. Joseph, Microglial subtypes: diversity within the microglial community, EMBO J. 38 (2019), e101997.
[55] X. Sun, S. Dong, H. Kato, J. Kong, Y. Ito, Y. Hirofuji, H. Sato, T.A. Kato, Y. Sakai, S. Ohga, S. Fukumoto, K. Masuda, Mitochondrial calcium-triggered oxidative stress and developmental defects in dopaminergic neurons differentiated from deciduous teeth-derived dental pulp stem cells with MFF insufficiency, Antioxidants (Basel) 11 (7) (2022) 1361.
[56] J. Takanashi, H. Oba, A.J. Barkovich, H. Tada, Y. Tanabe, H. Yamanouchi, S. Fujimoto, M. Kato, M. Kawatani, A. Sudo, H. Ozawa, T. Okanishi, M. Ishitobi, Y. Maegaki, Y. Koyasu, Diffusion MRI abnormalities after prolonged febrile seizures with encephalopathy, Neurology 66 (2006) 1304–1309 (discussion 1291).
[57] S. Tanaka, M. Ohgidani, N. Hata, S. Inamine, N. Sagata, N. Shirouzu, N. Mukae, S. O. Suzuki, H. Hamasaki, R. Hatae, Y. Sangatsuda, Y. Fujioka, K. Takigawa, Y. Funakoshi, T. Iwaki, M. Hosoi, K. Iihara, M. Mizoguchi, T.A. Kato, CD206 expression in induced microglia-like cells from peripheral blood as a surrogate biomarker for the specific immune microenvironment of neurosurgical diseases including glioma, Front. Immunol. 12 (2021), 670131.
[58] S.G. Utz, P. See, W. Mildenberger, M.S. Thion, A. Silvin, M. Lutz, F. Ingelfinger, N. A. Rayan, I. Lelios, A. Buttgereit, K. Asano, S. Prabhakar, S. Garel, B. Becher, F. Ginhoux, M. Greter, Early fate defines microglia and non-parenchymal brain macrophage development, Cell 181 (557–573) (2020), e518.
[59] P. Waters, G. Fadda, M. Woodhall, J. O'Mahony, R.A. Brown, D.A. Castro, G. Longoni, S.R. Irani, B. Sun, E.A. Yeh, R.A. Marrie, D.L. Arnold, B. Banwell, A. Bar-Or, N. Canadian Pediatric Demyelinating Disease, Serial anti-myelin oligodendrocyte glycoprotein antibody analyses and outcomes in children with Demyelinating syndromes, JAMA Neurol. 77 (2020) 82–93.
[60] M.E. Witte, D.J. Mahad, H. Lassmann, J. van Horssen, Mitochondrial dysfunction contributes to neurodegeneration in multiple sclerosis, Trends Mol. Med. 20 (2014) 179–187.
[61] Y. Yamaguchi, H. Torisu, R. Kira, Y. Ishizaki, Y. Sakai, M. Sanefuji, T. Ichiyama, A. Oka, T. Kishi, S. Kimura, M. Kubota, J. Takanashi, Y. Takahashi, H. Tamai, J. Natsume, S. Hamano, S. Hirabayashi, Y. Maegaki, M. Mizuguchi, K. Minagawa, H. Yoshikawa, J. Kira, S. Kusunoki, T. Hara, A nationwide survey of pediatric acquired demyelinating syndromes in Japan, Neurology 87 (2016) 2006–2015.
[62] L. Yang, M. Xie, M. Yang, Y. Yu, S. Zhu, W. Hou, R. Kang, M.T. Lotze, T.R. Billiar, H. Wang, L. Cao, D. Tang, PKM2 regulates the Warburg effect and promotes HMGB1 release in sepsis, Nat. Commun. 5 (2014) 4436.
[63] K. Zahra, T. Dey, S.P. Mishra Ashish, U. Pandey, Pyruvate kinase M2 and Cancer: the role of PKM2 in promoting tumorigenesis, Front. Oncol. 10 (2020) 159.
[64] I. Zanoni, R. Ostuni, L.R. Marek, S. Barresi, R. Barbalat, G.M. Barton, F. Granucci, J. C. Kagan, CD14 controls the LPS-induced endocytosis of toll-like receptor 4, Cell 147 (2011) 868–880.
[65] Y. Zhang, C.C. Boesen, S. Radaev, A.G. Brooks, W.H. Fridman, C. Sautes-Fridman, P.D. Sun, Crystal structure of the extracellular domain of a human fc gamma RIII, Immunity 13 (2000) 387–395.
[66] Y. Zhou, C. Cui, X. Ma, W. Luo, S.G. Zheng, W. Qiu, Nuclear factor kappaB (NF-kappaB)-mediated inflammation in multiple sclerosis, Front. Immunol. 11 (2020) 391.